GEOLOGICA CARPATHICA, AUGUST 2014, 65, 4, 257–271 doi: 10.2478/geoca-2014-0017

Distribution of elements among minerals of a single (muscovite-) biotite granite sample — an optimal approach and general implications

VOJTĚCH JANOUŠEK[1,2]✉, TOMÁŠ NAVRÁTIL[3], JAKUB TRUBAČ[1,2], LADISLAV STRNAD[4], FRANTIŠEK LAUFEK[1] and LUDĚK MINAŘÍK[3]

[1]Czech Geological Survey, Klárov 3/131, 118 21 Prague 1, Czech Republic;
✉vojtech.janousek@geology.cz; jakub.trubac@geology.cz; frantisek.laufek@geology.cz
[2]Institute of Petrology and Structural Geology, Charles University in Prague, Albertov 6, 128 43 Prague 2, Czech Republic
[3]Institute of Geology, Academy of Science, Rozvojová 269, 165 00 Prague 6, Czech Republic; navratil@gli.cas.cz; alex@gli.cas.cz
[4]Laboratories of the Geological Institutes, Charles University in Prague, Albertov 6, 128 43 Prague 2, Czech Republic;
ladislav.strnad@natur.cuni.cz

(Manuscript received January 17 2014; accepted in revised form June 5, 2014)

Abstract: The petrography and mineral chemistry of the coarse-grained, weakly porphyritic (muscovite-) biotite Říčany granite (Variscan Central Bohemian Plutonic Complex, Bohemian Massif) were studied in order to assess the distribution of major and trace elements among its minerals, with consequences for granite petrogenesis and availability of geochemical species during supergene processes. It is demonstrated that chemistry-based approaches are the best suited for modal analyses of granites, especially methods taking into account compositions of whole-rock samples as well as their mineral constituents, such as constrained least-squares algorithm. They smooth out any local variations (mineral zoning, presence of phenocrysts, schlieren…) and are robust in respect to the presence of phenocrysts or fabrics. The study confirms the notion that the accessory phases play a key role in incorporation of many elements during crystallization of granitic magmas. Especially the REE seem of little value in petrogenetic modelling, unless the role of accessories is properly assessed and saturation models for apatite, zircon, monazite±rutile carefully considered. At the same time, the presence of several P-, Zr- and LREE-bearing phases may have some important consequences for saturation thermometry of apatite, zircon and monazite.

Key words: modal analyses, trace-element residence, ICP-MS, Central Bohemian Plutonic Complex, Říčany granite.

Introduction

The distribution of chemical elements among minerals in a single granite specimen represents a fundamental and intriguing problem, which, however, has attracted surprisingly little attention in the current literature (e.g. Gromet & Silver 1983; Sawka 1988; Evans & Hanson 1993; Wark & Miller 1993; Bea 1996). Still, a good understanding of the net contributions of individual phases to the whole-rock chemical budget is a necessary prerequisite should any relevant petrogenetic modelling be undertaken. Moreover, particular host minerals show variable resistance to alteration and/or weathering, thus controlling the degree to which the given element could be mobilized into the environment.

For such studies, reliable and precise concentration data in small sample volumes are crucial. The data must be sufficient to minimize the effects of inhomogeneities in the analysed material (for individual minerals it could be the presence of zoning, inclusions, alteration zones…). The required precision is often far beyond the limits of the electron microprobe microanalysis (EMPA); the prohibitive cost effectively rules out the ion probe as well. Fortunately the ICP-MS technique enables a reliable determination of sub-ppm amounts of elements both in the solution (dissolved whole-rock powders or monomineralic separates) and *in situ*, using the laser-ablation (LA) apparatus.

In addition, an accurate estimate of the mineral modal proportions has to be made. Theoretically this should pose no problem, given that the modal analyses have provided a basis for classification of holocrystalline igneous rocks for over eighty years (Niggli 1931; Johannsen 1932, 1937, 1938, 1939; Streckeisen 1974; Le Maitre 2002).

The classical technique relies on counting of individual mineral grains over a regular grid, either in a standard thin section or a polished rock slab. More sophisticated alternatives include computer-aided image analysis, powder X-ray diffraction (P-XRD) and chemistry-based mathematical approaches (normative recalculations or statistical methods employing the chemistry of the bulk rock and its mineral constituents).

The current paper initially focuses on methodological issues connected with obtaining a modal analysis representative of a large, coarse-grained granite sample. The various methods are compared and the most trustworthy approach/modal data chosen (Appendix 1*). Then, using a combination of EMPA with (LA) ICP-MS data, an attempt is made to identify the principal mineral hosts for individual elements, evaluating the relative contributions of each of them to the whole-rock budget. Finally we discuss the general implications for obtaining modal analyses of coarse-grained rocks, modelling of igneous processes, obtaining reliable whole-rock trace-element analyses and saturation thermometry.

* — ***Appendices 1–5*** *(only as a Supplement in the electronical version; www.geologicacarpathica.com)*

Our case study concentrates on the Lower Carboniferous (Mississippian) Říčany (muscovite-) biotite granite pluton from the Central Bohemian Plutonic Complex (CBPC), Czech Republic (Fig. 1a). This small body is relatively well known, as it has been, over the years, a subject of numerous studies concerned with its geology, composition and genesis (e.g. Katzer 1888; Orlov 1933; Němec 1978; Palivcová et al. 1992; Janoušek et al. 1997; Trubač et al. 2009). Moreover, even more extensive research was done on element mobility during the weathering, mass fluxes, cycling and balance of elements within the model forest ecosystem (Minařík & Houdková 1986; Minařík & Kvídová 1986; Minařík et al. 1998, 2003; Navrátil et al. 2002, 2004, 2007). For both types of studies, detailed assessment of the elemental distribution among individual mineral phases has clearly been long overdue.

Geological setting

The CBPC is one of the largest composite granitoid complexes in the Central European Variscides (Fig. 1a). The individual petrographic types can be grouped into several suites, based on petrography, age, whole-rock and mineral geochemistry (Holub et al. 1997; Janoušek et al. 2000b; Žák et al. (2014) and references therein) (Fig. 1b). The oldest among them is the normal calc-alkaline *Sázava suite* (~355 Ma) forming much of the north-eastern CBPC. The most common in the central-southern CBPC are ~346 Ma old, K-rich calc-alkaline granodiorites to granites of the *Blatná suite* with minor basic bodies. The (ultra-) potassic *Čertovo břemeno suite* (~337 Ma) is formed by K-Mg-rich melagranites and melasyenites, the most basic types correspond-

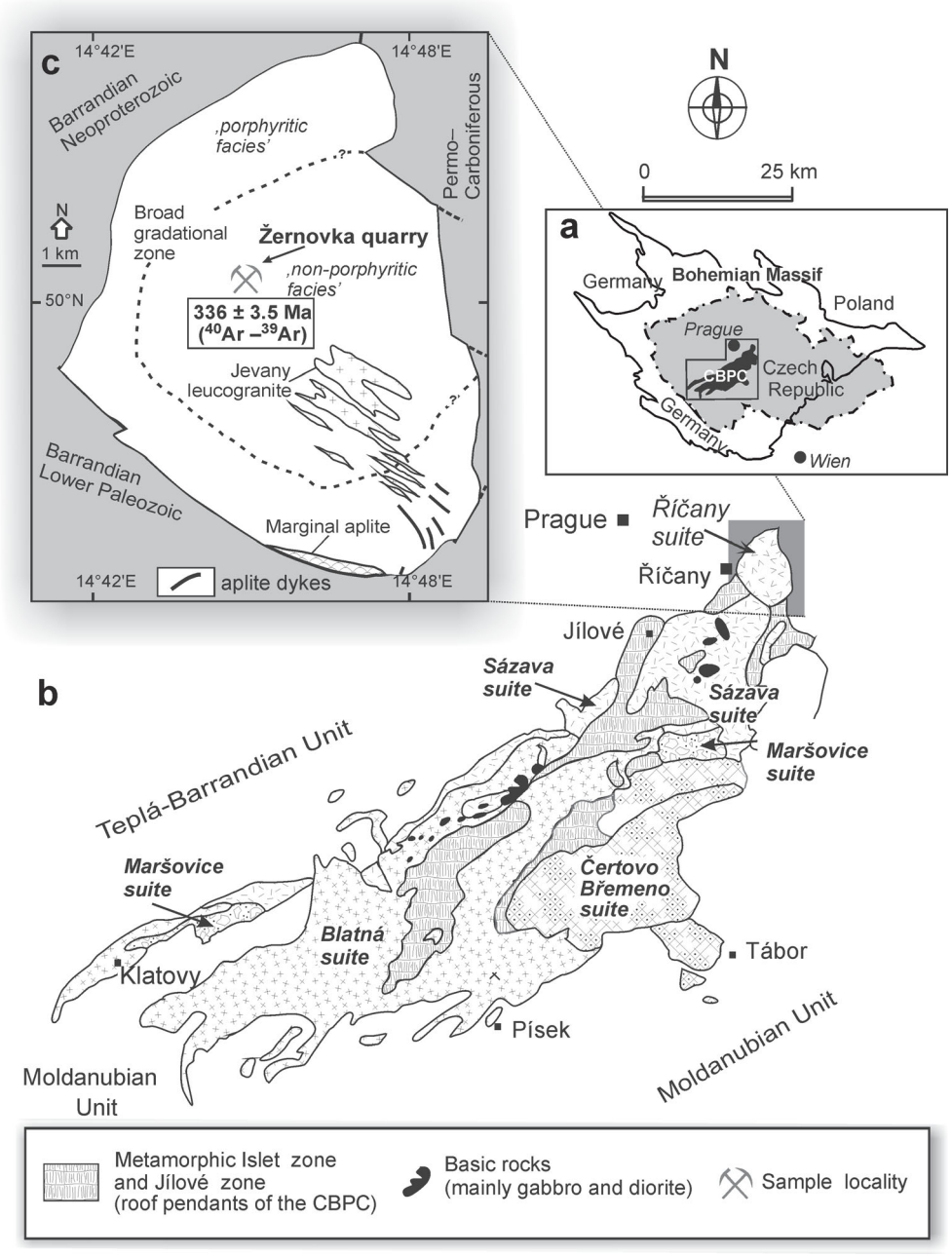

Fig. 1. a — Location of the Variscan Central Bohemian Plutonic Complex (CBPC) within the Bohemian Massif. **b** — Sketch of the CBPC with the main granitoid suites after Janoušek et al. (2000b) (normal calc-alkaline Sázava, high-K calc-alkaline Blatná, peraluminous Maršovice and (ultra-) potassic Čertovo břemeno). **c** — Geological outline of the Říčany Pluton and the surrounding units (after Janoušek et al. 1997). The position of the sampled locality, the working Žernovka quarry, is also indicated.

ing to the so-called durbachites. Strongly peraluminous Mu-Bt granodiorites (often Crd-bearing) of the *Maršovice suite* are regionally rather insignificant.

The Říčany Pluton (Fig. 1c), the main representative of the namesake suite, is a late (post-tectonic), shallow-level granitic body that has intruded the boundary between low-grade Upper Proterozoic to Lower Paleozoic metasediments of the Teplá–Barrandian Unit and dominantly high-grade metasediments of the Moldanubian Unit. Its eastern margin is obscured by Permo-Carboniferous sediments. The only modern geochronological information available is the ^{40}Ar–^{39}Ar biotite age of 336 ± 3.5 Ma (unpublished data of H. Maluski, cited in Janoušek et al. 1997).

The intrusion has a roughly elliptical outline (13×9 km) and is mainly made up of two distinct granite varieties. The outer, 'strongly porphyritic' one contains more abundant K-feldspar phenocrysts, whereas in the central, 'weakly porphyritic' facies, the phenocrysts are scarce (Katzer 1888) (Fig. 1c). The granite encloses numerous large biotite-rich mafic enclaves and less common metasedimentary xenoliths. The Pluton is cut by many pegmatite and aplite dykes. The central part has been intruded by several small bodies of fine-grained, equigranular, two-mica Jevany leucogranite and the southern exocontact is rimmed by the so-called Marginal aplite (Němec 1978).

Petrology and mineral chemistry

The studied rock comes from the central, 'weakly porphyritic' facies. It is relatively fresh, with the plagioclase showing limited argillitization along the cleavage planes (Fig. 2a). The scarce small K-feldspar phenocrysts are however slightly kaolinized and the biotite suffered incipient chloritization. The average grain size of the groundmass is 1–5 mm and rare phenocrysts may attain up to 3–5 cm. A completely unweathered sample of the granite was not available due to nowadays only limited quarry activity and widespread surface kaolinization of the pluton (Pivec 1969).

The *K-feldspar* phenocrysts are strongly perthitic and many show pronounced cross-hatched twinning; Carlsbad twins are also common. They contain numerous inclusions

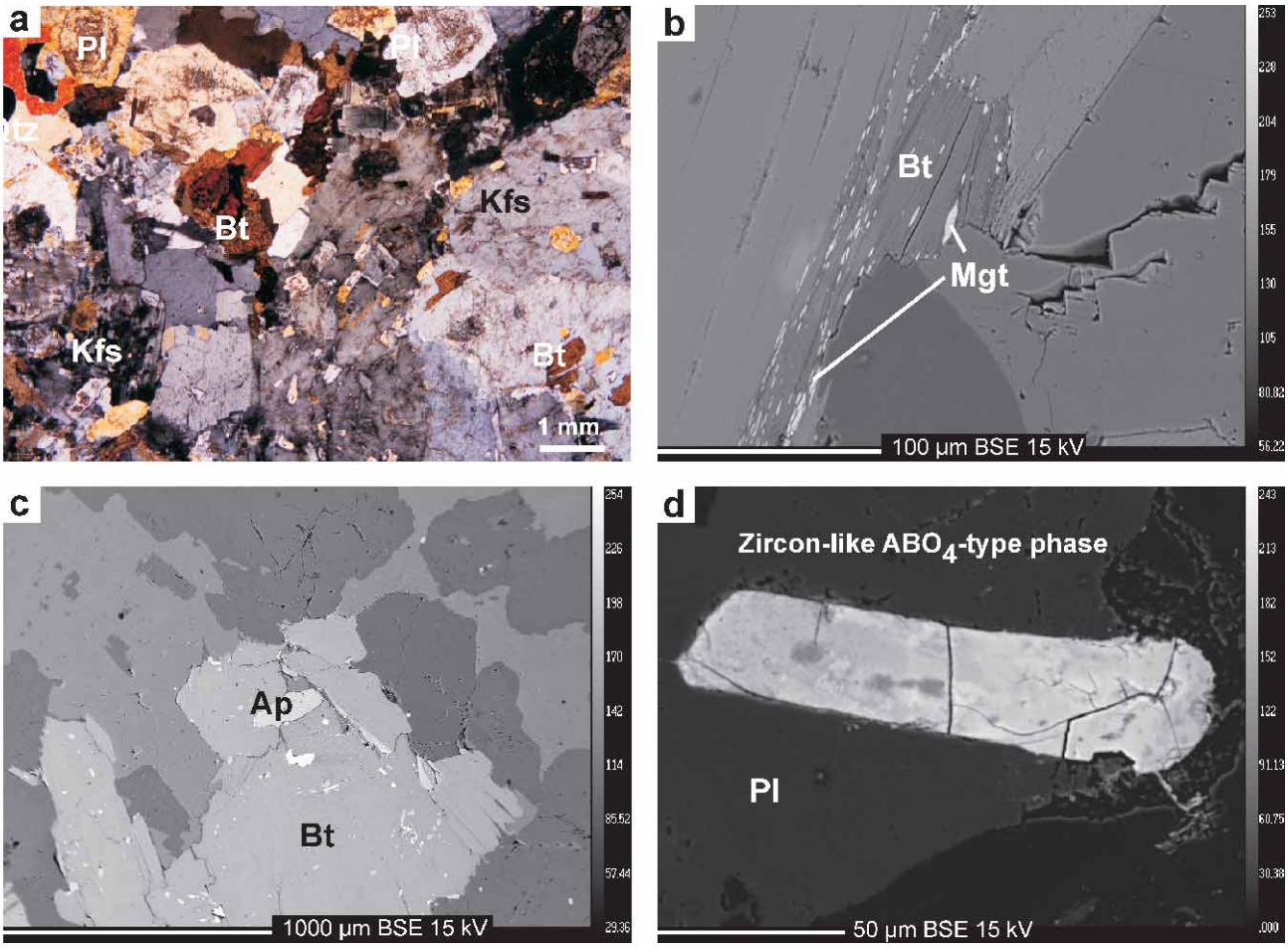

Fig. 2. Photomicrographs of the studied weakly porphyritic (muscovite-) biotite Říčany granite Žer-1. **a** — Photomicrograph of the typical magmatic texture at a rim of a small K-feldspar phenocryst with characteristic cross-hatched twinning. Crystals of the main rock-forming minerals exhibit no effects of solid-state deformation and are only slightly altered (plagioclase cores). Crossed polars. **b** — Back-scattered electron (BSE) image of micro-inclusions of magnetite in, and around, larger biotite flake. **c** — Typical BSE image of biotite, rich in apatite inclusions of variable shape and size. **d** — BSE image of the zircon-like ABO_4-type phase enclosed in plagioclase.

of biotite, quartz and oligoclase (an 'hourglass' texture of Pivec 1970).

Plagioclase occurs as subhedral prismatic crystals with common albite law twin lamellae, on average 1.2–2.0 mm across. Apart from those enclosed within the K-feldspar, they are of uniform oligoclase composition (An_{11-19}; Appendix 2) and are usually chemically unzoned.

Biotite forms subhedral flakes on average 0.5–0.75 mm (up to 1.2 mm) across, with a strong pleochroism: X — straw yellow, Y = Z — dark rusty-brown. Pleochroic haloes around submicroscopic inclusions are very distinct and common. Biotite is often associated with grains of magnetite (Fig. 2b).

Anhedral *quartz* grains with weak undulose extinction are up to 2 mm across.

The biotite may also be overgrown by scarce primary *muscovite* (up to 0.2 mm across). Also the plagioclase encloses some small (0.1–0.2 mm) flakes of muscovite, at least some of which appear to be of primary magmatic origin.

According to our microscopic and EPMA study and previous work of Kodymová & Vejnar (1974), the granite contains significant proportions of *rutile* (0.1 mm). Small *apatite* (0.1–0.2 mm) prisms or needles are often enclosed by biotite (Fig. 2c). Euhedral crystals of *titanite* (0.1 mm), brown to reddish in colour, and euhedral dipyramidal crystals of *zircon* (0.2 mm), pink to pale brown are less common accessories. *Monazite* (0.2 mm) usually occurs in forms aggregates of spherical grains. *Magnetite* (0.1 mm) occurs mostly in anhedral fragments, only rarely forming octahedra, up to 0.5 mm across. *Ilmenite* (0.1 mm) forms black opaque grains of non-metallic lustre, sometimes lamellated. Subangular hedral *zircon-like ABO_4-type phase* (up to 0.1 mm across) represents a newly encountered, rather rare accessory mineral. It occurs in plagioclase, very often together with monazite (Fig. 2d).

Modal proportions

Petrographic approaches

In the present case, both the conventional point counting and image analysis of the stained slab (Fig. 3a–b; see Appendix 1 for full analytical details on all methods used) were taken to approximate well the mineral proportions in the studied sample's matrix, as no sizeable K-feldspar phenocrysts are present in the hand specimen. The results do not differ greatly (Table 1). The image analysis (Fig. 3c–e) indicates somewhat higher amounts of biotite (9.0 vs. 7.3 vol. %: image analysis vs. conventional point counting, plagioclase (31.2 vs. 27.1 vol. %) and quartz (38.1 vs. 32.8 vol. %), at the expense of the K-feldspar (21.8 vs. 25.0 vol. %). Unfortunately the contents of kaolinite could not be determined by the image analysis. This mineral largely resisted staining and was thus counted, at least in part, as plagioclase.

Chemical methods

For sample Žer-1, the following mesonormative composition ('Improved Granite Mesonorm' of Mielke & Winkler 1979) is obtained (wt. %): Or 29.1, Pl (Ab + An) 36.8,

Table 1: Estimates of modal percentages (vol. % and wt. %, original data in bold) of the individual minerals in the Říčany granite Žer-1.

Mineral phase	Ideal formula	Density[1]	Point counting[2] (4890 points)		Image analysis		Granite mesonorm[3]		Constrained least-squares		X-ray diffraction (P–XRD)	
		($g.cm^{-3}$)	(vol. %)	(wt. %)	(vol. %)	(wt. %)	(vol. %)	(wt. %)	(vol. %)	(wt. %)	(vol. %)	(wt. %)
Main rock-forming minerals												
orthoclase	$KAlSi_3O_8$	2.570	**25.0**	24.4	**21.8**	21.2	30.0	**29.1**	28.7	**29.4**	29.6	**30.4**
plagioclase (albite)	$NaAlSi_3O_8$	2.620	**27.1**	26.9	**31.2**	30.9	37.2	**36.8**	36.3	**36.6**	25.0	**25.1**
kaolinite	$Al_2Si_2O_5(OH)_4$	2.594	**7.5**	7.4							1.2	**1.2**
biotite (F-phlogopite)	$KMg_3[AlSi_3O_{10}]F_2$	2.878	**7.3**	7.9	**9.0**	9.8	5.3	**5.8**	10.2	**9.3**	10.4	**9.5**
quartz	SiO_2	2.648	**32.8**	33.0	**38.0**	38.1	25.2	**25.2**	24.8	**24.7**	33.8	**33.8**
muscovite	$KAl_2[AlSi_3O_{10}](OH)_2$	2.831	**0.2**	0.2								
whole-rock		2.630										
Accessories			**0.1**	0.1								
ilmenite	$FeTiO_3$	4.788					0.2	**0.3**				
apatite	$Ca_5(PO_4)_3F$	3.200					0.3	**0.3**				
magnetite	Fe_3O_4	5.200					0.5	**0.9**				
sum			**100.0**	99.9	**100.0**	100.0	98.7	**98.4**	99.8	100.0	100.0	**100.0**

[1] – Data on mineral densities used in recalculation of wt. % to vol. % (or *vice versa*) are from Robie et al. (1967), whole-rock density of the Říčany granite from Hejtman (1948). Original data are in bold.

[2] – For explanation of the individual methods (point-counting, image analysis, least-squares calculation and XRD), see text. For more detailed outcome of the constrained least-squares method, see **Table 3.**

[3] – 'Improved Granite Mesonorm' of Mielke & Winkler (1979).

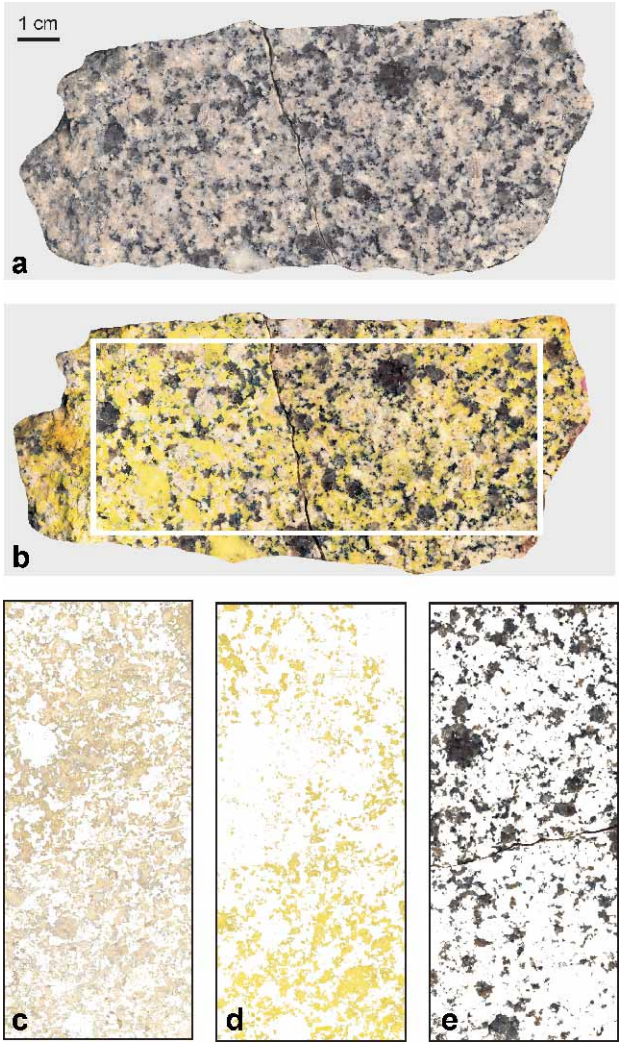

Fig. 3. Photograph of the polished hand specimen of the sample Žer-1, of natural appearance (**a**) and stained (**b**). The remaining images are separated colour components corresponding to the plagioclase (**c**) K-feldspar (**d**) and quartz with biotite (**e**). Box in figure (b) indicates the area used for image analysis (c–e).

Qtz 25.2, Bt 5.8, Ap 0.34, Mgt 0.9, Ilm 0.34, Cal 0.14 and Crn 0.54 (Table 1). The negligible proportion of normative corundum is in line with the subaluminous nature of the sample (A/CNK ~1.0 — Table 2). Normative calcite and corundum were further not considered as they do not correspond to mineral phases present in the rock.

The approximate proportions of the main rock-forming minerals (wt. %) were also obtained by the constrained least-squares (LSQ) method (Albarède 1995) implemented in the *GCDkit*. The whole-rock chemical composition and typical EMP analyses of the main rock-forming minerals served as an input (Table 3). Phosphorus, not present in appreciable amounts in any of the main phases but representing an essential structural component in two common accessories, apatite and monazite, was disregarded. The low sum of squared residuals (R^2=0.071) indicates an excellent fit. The proportions of K-feldspar (29.4 wt. %) and plagioclase (36.6 wt. %) are closely comparable to the mesonorm; but the quartz per-

SiO_2	70.34
TiO_2	0.36
Al_2O_3	14.64
Fe_2O_3	0.62
FeO	0.94
MgO	1.14
MnO	0.024
CaO	1.36
SrO	0.046
BaO	0.126
Li_2O	0.015
Na_2O	3.71
K_2O	5.55
P_2O_5	0.145
F	0.153
CO_2	0.06
C	0.016
S tot	<0.005
H_2O^+	0.51
H_2O^-	<0.05
F(ekv)	–0.064
S(ekv)	–0.001
Total	99.69
A/CNK	1.00
K_2O/Na_2O	1.50

Table 2: Whole-rock major- and minor-element analysis of the studied sample (wt. %).

A/CNK = molar $Al_2O_3/(CaO+Na_2O+K_2O)$ uncorrected for apatite.
K_2O/Na_2O ratio is given by weight.
For whole-rock trace-element composition, see Appendix 4.

Table 3: Constrained least-squares approximation to the modal composition (wt. %).

					Whole rock[2]			
	Plagioclase[1] Pl14	**K-feldspar Kfs1**	**Biotite Bt14**	**Quartz**	**Real**	**Estimated**	**Residual**	**Squared residual**
SiO_2	64.05	64.16	37.50	99.86	70.34	70.44	–0.10	0.010
TiO_2	0.00	0.00	3.33	0.00	0.36	0.31	0.05	0.002
Al_2O_3	21.76	18.47	14.80	0.02	14.64	14.78	–0.14	0.019
FeOt	0.04	0.03	17.26	0.00	1.50	1.64	–0.14	0.018
MnO	0.05	0.03	0.24	0.00	0.02	0.05	–0.02	0.001
MgO	0.00	0.00	13.35	0.00	1.14	1.25	–0.11	0.011
CaO	3.87	0.01	0.04	0.00	1.36	1.42	–0.06	0.004
Na_2O	9.42	0.96	0.14	0.00	3.71	3.75	–0.04	0.001
K_2O	0.40	15.61	9.47	0.00	5.55	5.61	–0.06	0.004
wt. %	36.6 %	29.4 %	9.3 %	24.7 %			R sqr	0.071[3]

[1] — Shown are real electron microprobe analyses of the main rock-forming minerals (see **Appendix 2**).
[2] — The observed whole-rock concentrations (**Table 2**) and the best estimate by the constrained least-squares method, with the corresponding differences (residuals).
[3] — The sum of squared residuals indicating a goodness of fit.

centage (24.7 wt. %) is somewhat lower (Table 1). The amount of biotite, however, is nearly double (9.3 wt. %) but much closer to estimates by point counting and image analysis (if recast to wt.%).

Powder X-ray diffraction (P-XRD)

The results of Rietveld quantitative phase analysis (Appendix 1) are summarized in Table 1 and Fig. 4. Compared with other methods, the plagioclase content is significantly underestimated (25.1 wt. %). The reason may be the complex preferred orientation of plagioclase, which shows two cleavage plane systems, namely [001] and [010], while only one correction for preferred orientation (for [001] direction) was applied in the Rietveld fit. The amount of K-feldspar (30.4 wt. %) is in agreement with the results of constrained LSQ (29.4 wt. %) and mesonorm (29.1 wt. %); while the quartz content is slightly higher (33.8 wt. %). The estimate of biotite (9.5 wt. %) is in line with other methods, except for the mesonorm. Clearly, the correction for preferred orientation in the [001] works sufficiently in this case. The content of kaolinite (1.2 wt. %) is significantly lower than that obtained by point counting (7.4 wt. %).

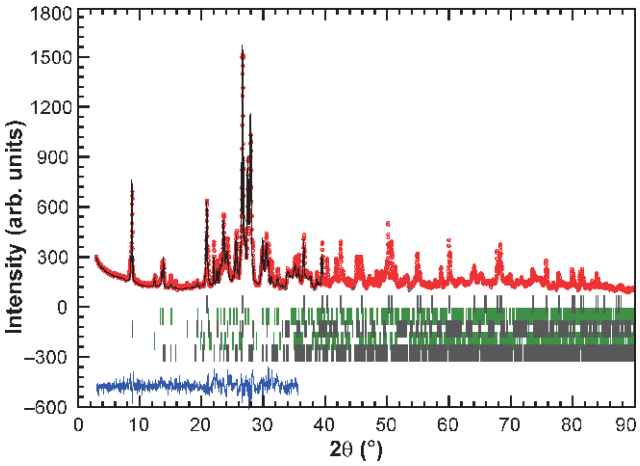

Fig. 4. Observed (circles), calculated (solid line) and difference Rietveld profiles for the studied sample. Markers of the peak positions (five rows of the vertical line segments) are for (from top to bottom) quartz, orthoclase, biotite, kaolinite and plagioclase.

Mineral chemistry

The compositions of individual minerals were analysed by a combination of three methods (Appendix 1), EMPA (see averages and typical analyses in Appendix 2), *in situ* LA ICP-MS and ICP-MS analyses of dissolved monomineralic separates (Appendix 3, summarized in Appendix 4). Laser-ablation analyses were preferred for mineral separates in which the presence of minor admixture of phases/inclusions with contrasting chemistry was of particular concern (quartz, plagioclase and biotite). On the other hand, wet analysis was chosen for K-feldspar, minimizing the problem of the small-scale heterogeneity (abundance of perthite lamellae). Fig. 5 shows selected trace-element patterns normalized by the whole-rock (WR) contents and Fig. 6 illustrates the chondrite-normalized REE patterns.

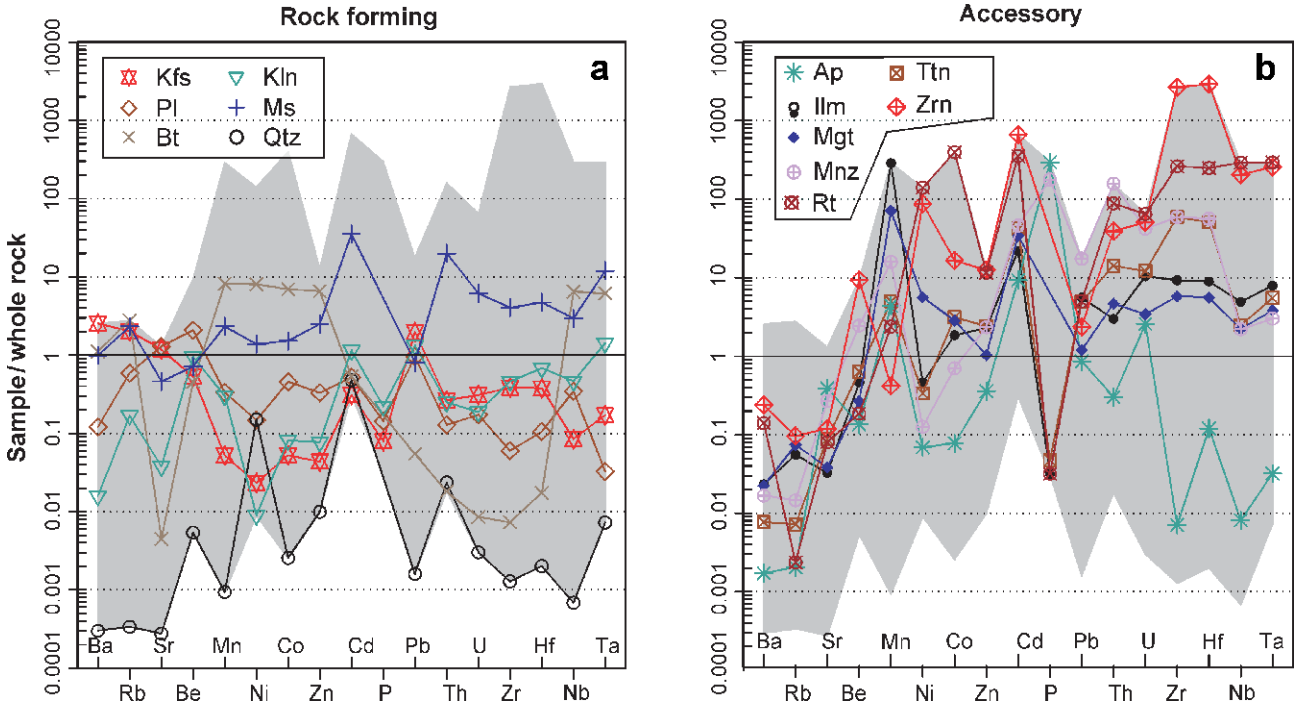

Fig. 5. Whole rock-normalized trace-element patterns for individual rock-forming (**a**) and accessory (**b**) minerals. Mineral abbreviations after Kretz (1983). Grey field denotes the total variation in the dataset.

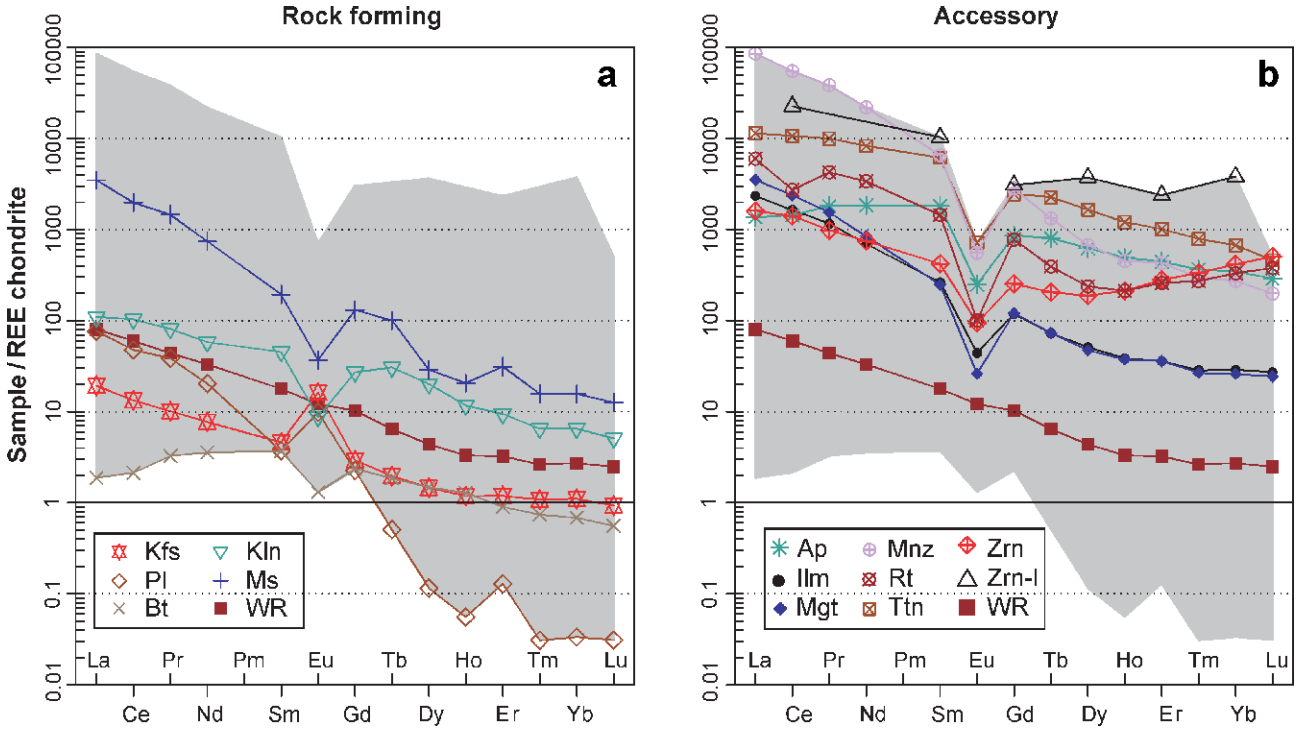

Fig. 6. Chondrite (Boynton 1984)-normalized REE spiderplots for the individual minerals. Zrn-l = zircon-like ABO_4-type phase. Grey field denotes the total variation in the dataset.

Feldspars and kaolinite

K-feldspar is characterized by roughly double enrichment of Ba, Rb and Pb over the whole-rock abundances; also Sr is slightly elevated (Fig. 5a). The *plagioclase* contains rather high Sr and Be (see Navrátil et al. 2002; Navrátil 2003). On the other hand, concentrations of transition metals and high field strength elements (HFSE) in both feldspars are very low. The *kaolinite* is stripped of much of the original K-feldspars' large-ion lithophile (LILE) budget, and contains only Cd, Pb and Ta in amounts exceeding those in the whole rock.

The *plagioclase* contains more than twice as much REE as the *K-feldspar* (81.3 vs. 26.6 ppm). Still the patterns are of similar shape, featuring a high degree of LREE over HREE enrichment and sizeable positive Eu anomalies (Fig. 6a). The feldspars share normalized Eu contents nearly identical to the whole rock but the concentrations of the remaining REE are significantly lower. The limited REE mobility in course of weathering of feldspars resulted in significantly higher apparent concentrations in the residual *kaolinite* (ΣREE ~191 ppm). Only Eu contents approach those of the host rock and thus the Eu anomaly turns to a strongly negative one.

Biotite and muscovite

The biotite is classified as phlogopite with 13.7–17.2 wt. % total Al_2O_3 (Al^{IV} 1.10–1.18 and Al^{VI} 0.16–0.27 apfu) and is relatively Mg-rich ($Mg/(Fe^T+Mg = 0.57–0.59$). The content of Al_2O_3 for muscovite is 31.3 wt. % total (Al^{IV} 1.44 and Al^{VI} 3.44 apfu). Both micas are slightly enriched in Rb, Mn (see Navrátil et al. 2007), Ni, Co, Zn, Nb and Ta. Elevated contents of Cd, Th, U, Zr and Hf are also characteristic of muscovite. The main differences lie in the total REE contents (7.3 ppm for biotite vs. 3396 ppm for muscovite). The muscovite REE pattern is steep, with a much higher degree of LREE/HREE enrichment compared to biotite (Fig. 6a). The Eu anomaly is negative in both cases.

Accessory minerals

Apatite: As shown by EMPA, the main minor constituents in apatite are Mn, Fe and Cl. It is further characterized by an enrichment of Mn, Cd and U (Fig. 5b). The Pb contents are close to those in the whole rock. Apatite is rich in REE, and the MREE in particular (ΣREE = 3962 ppm; Fig. 6b). A negative Eu anomaly is characteristic.

Zircon: This mineral is rather Hf poor (0.01–0.02 apfu) but contains high concentrations of other HFSE, such as Nb and Ta. Zircon is a major Cd, Zn, Ni and Co bearing-phase. High concentrations of U with Th are typical, as well as high ΣREE (2615 ppm) and parabolic, convex-up chondrite-normalized pattern with elevated HREE contents (Fig. 6b). While the Eu anomaly is negative, the Ce anomaly, typical of most igneous zircons (Hoskin & Schaltegger 2003), is absent. This, together with a rather low degree of HREE enrichment, might reflect the presence of inclusions (see fig. 1 in Hoskin & Schaltegger op. cit.) or an admixture of the zircon-like (Zrn-l) phase.

Monazite: Monazite shows large concentrations of P, Zr and Hf. Enrichment in radioactive elements is characteristic, with Th prevailing over U. Pb contents are also high. This mineral is enriched in REE, and especially LREE, with Ce

being the most abundant (ΣREE = 91,205 ppm; Fig. 6b). A deep negative Eu anomaly is characteristic.

Rutile: Rutile (TiO_2 > 98 wt. %) is a major transition metal-bearing phase (Ni, Co and Cd); it displays elevated U and Th contents. High HFSE concentrations (Zr, Hf, Nb and Ta) are also typical. It is a REE-rich mineral (ΣREE = 7358 ppm) with a fair degree of LREE/HREE fractionation and a deep negative Eu anomaly.

Ilmenite and magnetite: Both minerals are characterized by high contents of metals (Mn and Cd, less enriched Pb, Zn, Co and Ni) as well as HFSE. The U and Th contents are also somewhat elevated (Fig. 5b). The minerals are enriched in REE (ΣREE for ilmenite is 2735 ppm, for magnetite 3818 ppm), and the LREE in particular (Fig. 6b). The Eu anomaly is deeply negative in both cases.

Titanite: Titanite shows low Al (0.09–0.11 apfu) and Fe (0.03–0.03 apfu) contents. It is enriched in HFSE (Zr, Hf, Th and U, less so Nb and Ta). Elevated Cd contents are also typical. On the other hand, the LILE (Ba, Rb and Sr) are depleted compared to the whole rock (Fig. 5b). The ΣREE is high (21,314 ppm) and the REE pattern relatively steep (Fig. 6b) with a pronounced negative Eu anomaly.

Zircon-like ABO_4-type phase: The results of the EMPA of the zircon-like ABO_4-type phase are summarized in Appendix 5. Because of the relatively high Th contents, crystals are metamict and altered, and yield low analytical totals. The analysed phase appears to be a member of the zircon–thorite solid solution series (0.27–0.33 apfu Th, 0.49–0.55 apfu Zr), with substitution of Si by P (0.22–0.24 apfu) in the tetrahedral position B. The phase is highly enriched in Fe (0.03–0.23 apfu) and Ca (0.20–0.22 apfu. The Fe and Ca atoms, which probably enter the crystal structure during self-amorphization and interactions with circulating fluids, could be positioned in channels running parallel to the **c** axis of the crystal structure (Geisler et al. 2002, 2003). Silica removal accompanied by a hydration by post-magmatic, low-T fluids is also very probable.

Discussion

Modal analysis

Main rock-forming minerals

The choice of the most appropriate method for estimating modal abundances of the main rock-forming minerals was governed by comparison of the observed and calculated model whole-rock contents of the major- and minor-element oxides, as well as the most common among the LILE (Ba, Rb and Sr, which are hosted in granites mostly by feldspars and micas — Hanson 1978). Examining Fig. 7, it is clearly seen that the constrained LSQ method provides the most accurate estimate. As this approach does not give good assessments of contents of minor phases, no muscovite was included in the calculation and 0.2 wt. % of this mineral was added on the basis of the point counting. The 'best' modal proportions of the main rock-forming minerals are thus estimated to be: 0.365 Pl, 0.293 Kfs, 0.247 Qtz, 0.093 Bt and 0.002 Ms.

As for the rock classification in the QAP triangle (Fig. 8) (here essentially the vol. % of Kfs, Pl and Qtz recast to 1), the modal estimates by all methods yield comparable results and the studied rock classifies consistently as monzogranite. Still, the image analysis and, to some extent, point counting tend to overestimate somewhat the *Q* proportion, whereas the P-XRD approach results in a slightly lower *100*P/(A + P)* ratio of 47 % (other methods giving 55–59 %).

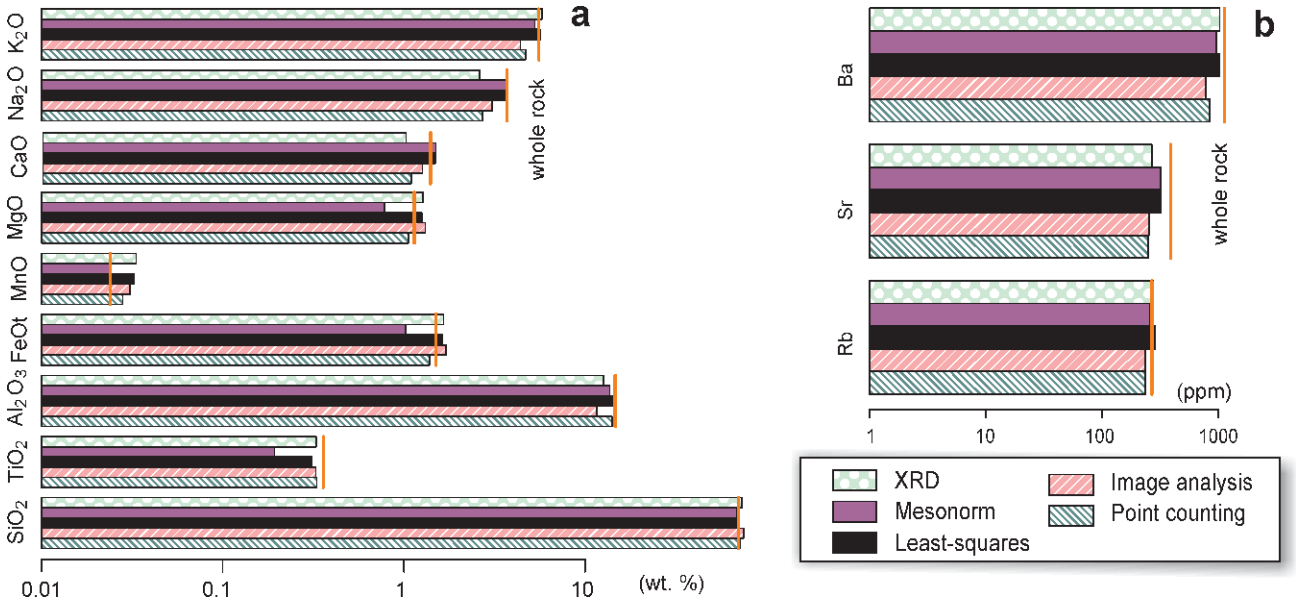

Fig. 7. Bar plots of calculated whole-rock contents of major- and minor-element oxides (**a**) and selected LILE (Rb, Sr and Ba) (**b**) calculated from representative mineral analyses (Appendices 2 and 4) and modal abundances estimated on the basis of the P-XRD, granite mesonorm, constrained least-squares (LSQ), image analysis of the stained thin slab and point counting of a standard thin section (Table 1). The best agreement with the whole-rock contents (vertical orange lines) is achieved by the LSQ method.

Accessory phases

After subtracting the elements hosted by the main rock-forming minerals (not only hosted incorporated in the lattice, but also contained in small inclusions, fluid inclusions or sorbed at grain boundaries, interfacial films etc.), the rest of the whole-rock chemical inventory has to be accounted for by the accessories. A crude estimate of a maximum modal abundance can be made using trace-element characteristics of the individual minerals. Assuming that such a phase accommodates the entire whole-rock inventory of the given element, these are as follows (Table 4, elements in brackets being the most restrictive ones): apatite <0.314 wt. % (P), monazite <0.046 wt. % (La), zircon <0.032 wt. % (Zr), rutile <0.081 wt. % (Nb), magnetite <1.121 wt. % (La) and titanite <0.255 wt. % (Y).

For some minerals, these constraints should approach the real modal abundances; the others contain no unique essential structural component, and instead share their trace-element load with other mineral phase(s). For instance, the maximal apatite content is likely to be overestimated, as part of P resides in monazite. Likewise, the LREE hosted in minerals other than monazite can hardly be neglected.

Regarding the opaque phases, ilmenite and magnetite are the possible carriers of the ferromagnetic properties in the granite. It is worth stressing that the mean magnetic susceptibility of the Říčany granite is low ($13.13–105.3\times10^{-6}$ [SI]: Trubač et al. 2009) and thus the rock must contain only a very limited amount of ferromagnetic component. Moreover, in the constrained LSQ calculation, the whole-rock Fe budget is exhausted by biotite and residual TiO_2 is as low as 0.05 wt. % (Table 3). According to petrographic investigation (Kodymová & Vejnar 1974), rutile seems to be the most important Ti-bearing accessory. Ilmenite, magnetite and titanite were therefore not taken into further consideration, in accordance with the microscopic and electron-microprobe studies showing all three phases to be rather rare. The modal abundance of the zircon-like ABO_4 phase remains unknown as the complete trace-element data are not available.

In order to assess the abundances of the remaining accessory minerals (Ap, Mnz, Zrn and Rt), the *unconstrained* LSQ method was applied to the outstanding trace-element inven-

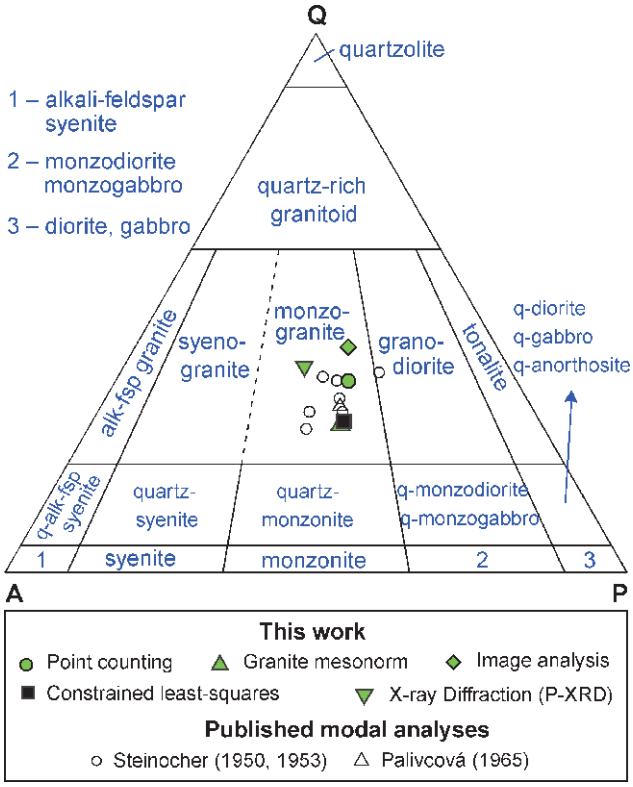

Fig. 8. QAP (quartz, K-feldspar, plagioclase) triangle of Streckeisen (1974) comparing previous modal analyses of the Říčany granite (Steinocher 1950, 1953; Palivcová 1965) with those obtained for sample Žer-1 in course of the present study by various methods. If necessary, the results were recast to vol. %.

Table 4: Maximum contents of selected accessory minerals (wt. %).

	Zr	Nb	La	Nd	Eu	Yb	Y	P	wt. %
Ap			2.875	1.166	1.431	0.661	0.473	**0.314**	0.314
Mnz	1.442	10.761	**0.046**	0.098	0.641	0.838	0.661	0.524	0.046
Zrn	**0.032**	0.116	2.459	2.882	3.780	0.550	1.240		0.032
Rt	0.327	**0.081**	0.655	0.634	3.543	0.691	1.391		0.081
Mgt	14.835	10.647	**1.121**	2.544	13.639	8.811	7.978		1.121
Ttn	1.443	9.563	0.343	0.260	0.498	0.340	**0.255**		0.255

Estimates are based on an assumption that the given mineral contains the full whole-rock inventory of the individual elements, after subtracting those hosted by the main phases (0.365 Pl, 0.293 Kfs, 0.247 Qz, 0.093 Bt and 0.02 Ms). Minima for each mineral are shown in bold; these represent maximum possible contents of each phase (last column).

Table 5: Modal percentages of the most abundant accessories (wt. %) estimated by the unconstrained least-squares method.

(ppm)	Ap[1]	Mnz	Zrn	Rt	Real[2]	Calc.[4]
Zr	1.2	10086.7	453122.0	44550.4	145.5	145.5
Nb	0.1	35.3	3288.9	4675.2	3.8	4.6
La	424.5	26574.3	496.4	1861.8	12.2	13.5
Nd	1105.0	13148.3	446.9	2031.7	12.9	10.2
Eu	18.3	40.8	6.9	7.4	0.3	0.1
Yb	72.2	57.0	86.9	69.1	0.5	0.3
Y	1173.8	839.3	447.3	398.7	5.5	4.2
P	186228.0	111734.2	0.0	17.5	585.4	585.4
Estimated modal proportions (wt. %)[3]	0.290 %	0.040 %	0.023 %	0.082 %		

[1] — Real mineral analyses are summarized in the **Appendix 2.**

[2] — The whole-rock composition not accounted for by the main rock-forming minerals. See text for discussion.

[3] — Estimated modal percentages obtained by the least-squares approach.

[4] — Composition of a mixture (ppm) calculated using these mineral proportions.

wt. %	Or 29.178	Pl 36.379	Qtz 24.527	Bt 9.285	Ms 0.199	Ap 0.289	Mnz 0.04	Zrn 0.023	Rt 0.081	wt. %
SiO_2	18.72	22.91	24.49	3.48	0.1			0.01		69.71
TiO_2				0.31					0.08	0.39
Al_2O_3	5.39	7.8		1.37	0.06					14.12
FeOt	0.01			1.6	0.01					1.62
MnO	0.01			0.02						0.03
MgO				1.24						1.24
CaO		1.44				0.16				1.60
Na_2O	0.28	3.35		0.01						3.64
K_2O	4.55	0.16		0.88	0.02					5.61
P_2O_5		0.01				0.12	0.01			0.14
ppm										
Rb	156.56	57.2	0.02	68.64	1.23			0.01		283.66
Sr	133.84	181.91	0.03	0.16	0.36	0.43	0.04	0.01	0.02	316.80
Ba	832.34	49.31	0.08	116.33	2.21	0.01	0.01	0.06	0.13	1000.48
Ni	0.1	0.77	0.53	10.72	0.04			0.29	1.63	14.08
Co	0.05	0.58		2.28	0.01			0.01	1.13	4.06
Zn	0.5	4.75	0.1	24.14	0.2	0.04	0.04	0.12	0.37	30.26
Cd	0.01	0.02	0.01	0.01	0.01			0.02	0.03	0.11
Be	1.61	7.88	0.01	0.44	0.02		0.01	0.02		9.99
Pb	36.39	21.95	0.02	0.32	0.1	0.16	0.44	0.04	0.26	59.68
Th	1.88	1.14	0.14	0.04	0.96	0.02	1.52	0.22	1.75	7.67
U	0.87	0.6	0.01	0.01	0.12	0.07	0.16	0.11	0.5	2.45
La	1.74	8.63		0.05	2.14	1.23	10.54	0.11	1.51	25.95
Ce	3.13	14		0.16	3.17	3.34	17.55	0.26	1.79	43.40
Pr	0.36	1.71		0.04	0.35	0.64	1.85	0.03	0.42	5.40
Nd	1.35	4.45		0.2	0.89	3.19	5.21	0.1	1.65	17.04
Sm	0.26	0.26		0.07	0.08	1.02	0.51	0.02	0.23	2.45
Eu	0.35	0.26		0.01		0.05	0.02		0.01	0.70
Gd	0.22	0.21		0.06	0.07	0.64	0.29	0.02	0.16	1.67
Tb	0.03	0.01		0.01	0.01	0.11	0.02		0.02	0.21
Dy	0.14	0.01		0.04	0.02	0.58	0.09	0.01	0.06	0.95
Ho	0.02			0.01		0.1	0.01		0.01	0.15
Er	0.07	0.01		0.02	0.01	0.27	0.04	0.01	0.04	0.47
Tm	0.01					0.03			0.01	0.05
Yb	0.07			0.01	0.01	0.21	0.02	0.02	0.06	0.40
Lu	0.01					0.03			0.05	0.01
Y	0.71	0.05		0.26	0.07	3.39	0.33	0.1	0.32	5.23
Nb	0.4	2.02		9.65	0.09		0.01	0.76	3.8	16.73
Ta	0.08	0.02		0.94	0.04			0.1	0.39	1.57
Zr	19.01	3.71	0.05	0.12	1.37		4	104.86	36.21	168.83
Hf	0.6	0.21		0.01	0.05		0.12	3.69	1.11	5.79

Fig. 9. Balloon plot (Jain & Warnes 2006) expressing the balance of individual elements in the studied granite sample. The relative contributions of individual minerals are expressed by the colour and size of circles plotted. Each number was obtained by multiplication of the particular element/oxide concentration within the given mineral and the best estimate of its modal abundance. The goodness of fit could be assessed comparing row totals with the real whole-rock analyses.

tory. Trace elements which often represent their essential structural components (Zr, Nb, La, Nd, Eu, Yb, Y and P) were selected. In the solution (Table 5), Ap dominates (0.29 wt. %) over Rt (0.082 %), Mnz (0.04 %) and Zrn (0.023 %). The results are feasible as all obey the upper limits (Table 4) and the residuals for all modelled elements are satisfactory.

Whole-rock geochemical budget

Total balance

The overall balance of individual elements in the studied sample is illustrated by means of the balloon plot (Jain & Warnes 2006). This diagram conveys important aspects of tabular data without obscuring the exact numerical values (Fig. 9, see caption for explanation of the principle). For the trace elements, the final balance is also presented as an upper continental crust (Taylor & McLennan 1995) normalized spiderplot (Fig. 10). Here, both the real concentrations and computed abundances match rather well. Only middle-heavy REE and, most notably, Th and U are strongly underestimated, suggesting the presence of an additional, U,Th, HREE-rich phase not accounted for in our model. The obvious candidate is the zircon-like ABO_4 mineral (Appendix 5; Fig. 6b), the role of which could not be quantified as we do not have information on its modal percentage and most of the trace-element signature. Its mean concentrations of Th, U and Yb nevertheless correspond to ~27,000, >3500 and >350× those found in the upper continental crust (Taylor & McLennan 1995).

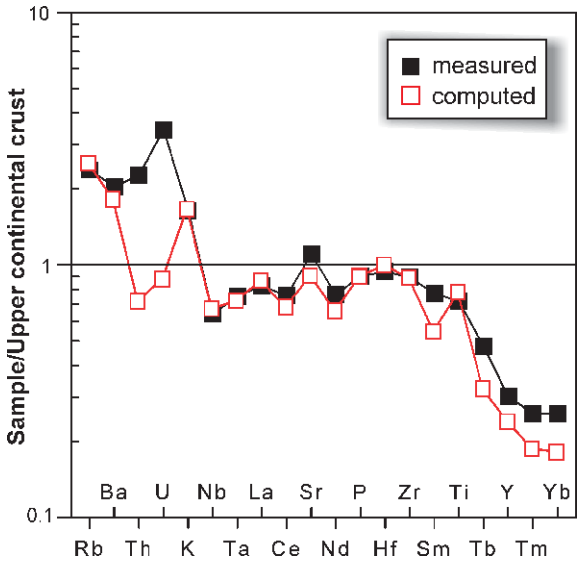

Fig. 10. Spiderplot of trace-element concentrations observed in the whole-rock sample Žer-1 (filled squares) and calculated (empty squares), normalized by abundances in the average upper continental crust (Taylor & McLennan 1995). The calculation was made for all the minerals present in Fig. 9.

Residence in individual minerals

Returning to Fig. 9, one can examine the residence of particular elements in detail. Silica is hosted almost equally by quartz (35 wt. % of its whole-rock abundance), plagioclase (33 %), and somewhat less by K-feldspar (27 %). Bulk Ti, Fe and Mg are held by biotite, whereby rutile contains a fifth of the whole-rock TiO_2. Much of the MnO is also accounted for by biotite but almost a third is hosted by K-feldspar. As expected, the main reservoirs for Al_2O_3 are the feldspars (Pl: 52 %, Kfs: 38 %). Surprisingly little Al, however, resides in biotite (10 %), owing to its small modal abundance. Most of the CaO and Na_2O are bound to plagioclase (~90 %); only 10 % of the former is stored in apatite and 8 % of the latter in K-feldspar. Part of the Na_2O contents in K-feldspar is to be ascribed to small plagioclase inclusions observed during petrographic studies. For K_2O, K-feldspar is clearly the key host (81 %), biotite accounting for a mere 16 % of the whole-rock budget. The main reservoir for P is apatite; monazite's contribution is small, close to 7 %.

Concerning the LILE, Rb is accumulated by K-feldspar (55 %), biotite comes second (24 %) and plagioclase third (20 %). The two feldspars represent almost equally important Sr reservoirs (Pl: 57 %, Kfs: 42 %). The bulk of Ba is concentrated in K-feldspar (83 %); both biotite (12 %) and plagioclase (5 %) are rather unimportant. The overwhelming majority of Be (79 %) is located in plagioclase; K-feldspar and biotite share the rest. Lead is another element for which the feldspars are the main hosts (Kfs: 61 %, Pl: 37 %).

The most important LREE reservoirs are monazite (41 % La) and plagioclase (33 % La), while muscovite, K-feldspar, rutile and apatite seem to be much less significant. The bulk of Eu is accounted for by the feldspars (Kfs: 50 % and Pl: 38 %); the apatite contribution represents a mere 8 %. On the other hand, apatite is the most important host for the middle and heavy REE as well as Y. Less significant HREE-bearing phase is rutile. Surprisingly, zircon and monazite do not rank among important sinks for HREE, owing to their scarcity.

Regarding the radioactive elements, both feldspars seem to incorporate much U (Kfs: 35 and Pl: 25 %). Among accessories, rutile accounts for over 20 % of both Th and U. Almost equally significant for Th are K-feldspar, monazite and rutile, less so plagioclase (15 %) and muscovite (13 %). Minerals such as zircon and apatite play only marginal roles in hosting the radioactive elements, unlike probably the newly recognized zircon-like ABO_4 phase, even though its role cannot be quantified.

Among the HFSE, the zircon contains only ~70 % of the total Zr and Hf; with rutile accounting for the rest. About 60 % of the Nb and Ta budget are hosted by biotite. We can only speculate that this may be in the form of submicroscopic inclusions; for rutile remains approximately one fifth of the whole-rock inventory.

General implications

Modal analysis

Petrographic techniques: In studies of granitic rocks, unstained thin sections are best suited for most textural observations, as well as description of optical properties and identification of mafic minerals. In many cases, however, it is difficult to determine some of the colourless phases, particularly if the feldspars are not twinned or their grains are small. One way out is to use cold-stage cathodoluminescence (CL), in which the (mostly) blue K-feldspars are easily distinguished from ochre–yellow plagioclases and almost non-luminescent quartz (Marshall 1988; Janoušek et al. 2000a, 2004). CL also facilitates rapid determination and mapping of some accessory phases, such as of apatite, monazite and zircon. Nowadays largely neglected, staining turns K-feldspars yellow and plagioclase white, also facilitating point counting (Gabriel & Cox 1929; Hollocher 2013).

Obtaining a statistically valid modal analysis by point counting of a standard thin section can be troublesome, especially for coarse-grained or porphyritic rocks (Chayes & Fairbairn 1951; Chayes 1954, 1965; Hutchison 1974). In order to maximize the counted area in these cases, it was proposed to use rock slabs or point count directly on the outcrop (e.g. Hutchison 1974) — but such methods are cumbersome and seldom used. Clearly, the situation becomes even more complicated when the rock possesses a fabric, as one deals essentially with a 2D section of a three-dimensional anisotropic body.

In our case, the approach using the stained polished slab is superior, as it represents an area larger than the standard section (ca. 119 vs. 6 cm^2). The current work confirms that the tedious point-counting of the stained sample can be successfully replaced by computer-aided image analysis. However, this method also brings about some new problems, for example, some degree of ambiguity caused by alteration of the feldspar.

P-XRD: The Rietveld method has been widely used for quantitative phase analysis of various geological materials and industrial products (Madsen & Scarlett 2009 and references therein). This full-pattern profile fitting method has several advantages over other diffraction approaches to quantitative phase analysis using at most a few of the strongest reflections from each phase in the mixture (Bish & Post 1989). Nevertheless, the application of the Rietveld method to geological materials still poses significant problems. The most pronounced difficulties are micro-absorption effects, complex preferred orientation, various chemical substitutions in minerals and also the presence of structural defects.

Our estimate of modal composition obtained by P-XRD is probably biased by the defective structure of kaolinite, which is affected by planar disorder. Considering the complexity of the diffraction pattern, the large number of reflections and presence of significant preferred orientation, the results from P-XRD are reasonable, in other words they are comparable to other approaches. The advantage of the P-XRD method over standard petrographic techniques is that it represents, like the chemical approaches, the whole volume of the homogenized sample.

Chemical methods: For the sample Žer-1, the bulk-rock analysis represents ~30 kg, or over 11,000 cm^3 of the rock, and thus should be robust to the presence of fabrics, phenocrysts and local inhomogeneities such as schlieren. Major-element or norm-based schemes (Streckeisen & Le Maitre

1979; De La Roche et al. 1980; Debon & Le Fort 1988) have been preferred by many authors for classification purposes. However, some normative recalculations involve minerals not encountered in common felsic plutonites and thus their use is not straightforward (e.g. CIPW and Catanorm — Hutchison 1975). For this reason, Mielke & Winkler (1979) developed their 'Improved Mesonorm', designed specifically for granitic rocks.

With the spread of personal computers, mathematical methods became popular. They attempt to find the best estimate of modal proportions based on major- and minor-element analyses of the large whole-rock sample and its typical mineral constituents. As usually the number of chemical components exceeds that of the mineral phases, there is no unique solution and the algorithms rely on the least-squares or linear programming approaches (e.g. Wright & Doherty 1970; Le Maitre 1981; Laube et al. 1996; Paktunc 1998; Janoušek et al. 2006). Potential pitfalls could lie in the choice of typical mineral compositions and/or the weathering/alteration effects. The methods are also rather insensitive to the presence of minor/or accessory phases, whose contents have to be assessed separately.

Here the results obtained by mesonormative and LSQ approaches are closely comparable for felsic minerals (Fig. 8). The amount of biotite, however, is nearly half (5.8 vs. 9.3 wt. %, respectively), and much lower also than estimates by the remaining methods. The reason probably lies in the fact that the mesonorm also estimates the proportion of magnetite and ilmenite, whereby in the LSQ calculation the sole iron-bearing phase is biotite. The normative contents of the opaque phases seem overestimated by the mesonormative algorithm, especially that of magnetite (0.9 %).

Taken together, several of the methods employed here to estimate the modal proportions of the main rock-forming minerals have yielded comparable results. It is necessary to stress that the current case is a particularly favourable one, as no significant zoning of mineral phases, not even of plagioclase, has been observed in the Říčany Pluton. Moreover, K-feldspar phenocrysts in the studied sample are small and sparse. Still, the constrained LSQ method (Albarède 1995) was found superior to all other approaches. The obtained percentages of the main rock-forming minerals compare well with the modal analyses determined previously by conventional point counting (Steinocher 1950, 1953; Palivcová 1965) (Fig. 8).

Petrogenetic modelling

Collectively, the four accessories, apatite, monazite, zircon and rutile host more than half of the total LREE and over three quarters of the HREE + Y, Zr and Hf of the studied granite sample. The cases of Th, U, Ti, Ni, Co, Nb and Ta are similar, albeit not so extreme. This confirms the notion that the accessories are often crucial in controlling the behaviour of many elements in granitic systems (e.g. Mittlefehldt & Miller 1983; Miller & Mittlefehldt 1984; Bea 1996). Particularly the REE are of little value in petrogenetic modelling of fractional crystallization of the main rock-forming minerals, unless the role of accessories is properly assessed.

Determination of the whole-rock trace-element abundances

Some 10–30 % of the whole-rock HREE, U, Th, Nb, Ta, Ti, Cd, Co and Ni, and even more of Zr and Hf, are contained in the resistant accessories, zircon and rutile. Thus the pressure bomb or sample fusion are absolutely essential in sample decomposition, if these elements are to be determined quantitatively (e.g. Potts 1987; García de Madinabeitia et al. 2008 and references therein). Using a combined HF, HCl and HNO_3 attack is clearly inadequate and will induce low total REE contents and artificially increased degrees of LREE/HREE fractionation. Alas such cases are by no means rare — for instance, the acid decomposition casts serious doubts on some of the results by Minařík et al. (1998).

Saturation thermometry

Our study provides some interesting implications for the accessory phase saturation thermometry commonly used in the granite studies (see Janoušek 2006 and Anderson et al. 2008 for review). As in Říčany phosphorus is hosted nearly exclusively by apatite (86 % of the whole-rock contents), the saturation thermometry involving this mineral should apply be applicable. Indeed the temperature calculated for the uncorrected whole-rock P_2O_5 content and that based on apatite-hosted P_2O_5 are both mutually closely comparable (946 vs. 931 °C according to the model of Harrison & Watson 1984). The fact that they are unrealistically high for a granitic magma can be related to the sensitivity of the algorithm to exact determinations of P_2O_5 contents, as the isotherms converge rapidly for increasingly acidic compositions (see fig. 3a in Janoušek 2006).

Zircon incorporates a mere 62 % of the whole-rock Zr budget (Fig. 9), the rest being hosted by other phases, most importantly the early crystallizing rutile. The zircon saturation thermometry (Watson & Harrison 1983) thus yields a liquidus temperature estimate (784 °C) ca. 40 °C higher than that calculated for the corrected Zr concentration.

The case of monazite is more complex, though. The model of Montel (1993) includes additional parameters apart from the temperature, major-element and LREE contents of the magma. One is the fraction of REE phosphates in the monazite but this can be directly measured (the average for Říčany monazite is 89.5 mol %). More difficult to constrain are the water contents of the magma. Fortunately, the effect is not great (738 °C is obtained for 3 wt. % H_2O; 761–724 °C for 1–5 wt. % H_2O).

Plagioclase represents an important sink for LREE, with monazite containing some 21–41 % of the whole-rock inventory. This brings problems for the LREE-based monazite thermometry. While the uncorrected LREE content yields 738 °C, the corrected content gives barely 668 °C, that is about 70 °C less (for 3 wt. % H_2O in the magma melt). Such a corrected temperature seems to be too low for a granitic magma. However, one should take into account the petrological evidence indicating that the monazite saturation level was probably reached early, prior to the onset of the plagioclase crystallization. Thus using the uncorrected temperature seems more justifiable here.

Conclusions

The study of the petrography and mineral chemistry of a single large sample of coarse-grained, weakly porphyritic (muscovite-) biotite granite from the Říčany intrusion (Czech Republic) has yielded the following conclusions:

1. The methods taking into account the whole-rock composition as well as the true mineral chemistries (linear programming or constrained least squares) are particularly suitable for modal analyses of granitic rocks. The modes then represent a large volume of sample and thus (i) smooth out any local variations, such as small-scale crystal accumulation, (ii) account for the presence of phenocrysts, and (iii) are insensitive to shaped-preferred orientation/fabric.

2. Accessory phases control the behaviour of many trace elements in differentiation of felsic granitic systems. Clearly the REE are of little value in petrogenetic modelling of the main rock-forming minerals fractionation, unless the role of accessories is properly assessed and existing saturation models for apatite, zircon, monazite ± rutile are carefully considered.

The fact that many of the essential structural components (P, Zr, LREE) used in apatite, zircon and monazite saturation thermometry are incorporated into other minerals may lead to significant overestimation of the liquidus temperatures. In the present case, the saturation temperatures for zircon would be overestimated as ca. 40 °C due to significant contents of Zr in the early crystallized rutile. However, the correction for monazite (–70 °C) probably should not be applied as most of the extra LREE are hosted by plagioclase, a relatively late mineral.

In the studied sample, over 80 % of the whole-rock Zr and Hf and ca. 10–30 % of HREE, U, Th, Nb, Ta, Ti, Cd, Co and Ni are contained in resistant accessory phases Zrn and Rt. Thus the pressure vessel or sample fusion — and not merely a combined acid attack — are absolutely essential in sample decomposition if these elements are to be determined quantitatively.

Acknowledgments: This manuscript benefited from insightful comments by I. Broska, an anonymous reviewer and handling editor I. Petrík, as well as from careful editing by E. Petríková. The authors are indebted to Z. Korbelová for assistance at the electron microprobe and J.K. Novák (both Geological Institute, Czech Academy of Sciences, Prague — GLI) who carried out the point counting analysis. V. Sedláček (GLI) did the mineral separations, P. Hasalová (Czech Geological Survey) helped with staining of feldspars. Janoušek and Trubač acknowledge the support by the Grant Agency of the Czech Republic (GAČR, No. P210/11/1168) and Czech Ministry of Education, Youth and Sports (Project LK 11202); Minařík and Navrátil were supported from institutional Project No. RVO67985831. This study is a part of the Ph.D. research of Jakub Trubač.

References

Albarède F. 1995: Introduction to geochemical modeling. *Cambridge University Press*, Cambridge, 1–543.

Anderson J.L., Barth A.P., Wooden J.L. & Mazdab F. 2008: Thermometers and thermobarometers in granitic systems. In: Putirka K.D. & Tepley III F.J. (Eds.): Minerals, inclusions and volcanic processes. *Mineral. Soc. Amer.; Geochem. Soc. Rev. Miner. Geochem.,* Washington 69, 121–142.

Bea F. 1996: Residence of REE, Y, Th and U in granites and crustal protoliths; implications for the chemistry of crustal melts. *J. Petrology* 37, 521–552.

Bish D.L. & Post J.E. 1989: Modern powder diffraction. *Mineral. Soc. Amer. Rev. Miner.,* Washington 20, 1–369.

Boynton W.V. 1984: Cosmochemistry of the rare earth elements: meteorite studies. In: Henderson P. (Ed.): Rare earth element geochemistry. *Elsevier*, Amsterdam, 63–114.

Chayes F. 1954: The theory of thin-section analysis. *J. Geol.* 62, 92–101.

Chayes F. 1965: Reliabilty of point counting results. *Amer. J. Sci.* 263, 719–724.

Chayes F. & Fairbairn H.W. 1951: A test of the precision of thin-section analysis by point counter. *Amer. Mineralogist* 36, 704–712.

Debon F. & Le Fort P. 1988: A cationic classification of common plutonic rocks and their magmatic associations: principles, method, applications. *Bull. Minéral.* 111, 493–510.

De La Roche H., Leterrier J., Grandclaude P. & Marchal M. 1980: A classification of volcanic and plutonic rocks using R_1R_2-diagram and major element analyses — its relationships with current nomenclature. *Chem. Geol.* 29, 183–210.

Evans O.C. & Hanson G.N. 1993: Accessory-mineral fractionation of rare-earth element (REE) abundances in granitoid rocks. *Chem. Geol.* 110, 69–93.

Gabriel A. & Cox E.P. 1929: A staining method for the quantitative determination of certain rock minerals. *Amer. Mineralogist* 14, 290–292.

García de Madinabeitia S., Sánchez Lorda M.E. & Gil Ibarguchi J.I. 2008: Simultaneous determination of major to ultratrace elements in geological samples by fusion-dissolution and inductively coupled plasma mass spectrometry techniques. *Anal. Chim. Acta* 625, 117–130.

Geisler T., Pidgeon R.T., van Bronswijk W. & Kurtz R. 2002: Transport of uranium, thorium, and lead in metamict zircon under low-temperature hydrothermal conditions. *Chem. Geol.* 191, 141–154.

Geisler T., Pidgeon R.T., Kurtz R., van Bronswijk W. & Schleicher H. 2003: Experimental hydrothermal alteration of partially metamict zircon. *Amer. Mineralogist* 88, 1496–1513.

Gromet L.P. & Silver L.T. 1983: Rare earth element distribution among minerals in a granodiorite and their petrogenetic implications. *Geochim. Cosmochim. Acta* 47, 925–939.

Hanson G.N. 1978: The application of trace elements to the petrogenesis of igneous rocks of granitic composition. *Earth Planet. Sci. Lett.* 38, 26–43.

Harrison T.M. & Watson E.B. 1984: The behavior of apatite during crustal anatexis: equilibrium and kinetic considerations. *Geochim. Cosmochim. Acta* 48, 1467–1477.

Hejtman B. 1948: Directory of quarries in Czechoslovakia, No. 26, Český Brod. [Soupis lomů ČSR, č. 26, okres Český Brod.] *SGÚ ČSR*, Praha, 1–71 (in Czech).

Hollocher K. 2013: Staining feldspars in thin section. Accessed on 23 December 2013 at *http://minerva.union.edu/hollochk/c_petrology/staining_feldspars.htm*

Holub F.V., Machart J. & Manová M. 1997: The Central Bohemian Plutonic Complex: geology, chemical composition and genetic interpretation. *Sbor. Geol. Věd, ložisk. Geol. Mineral.* 31, 27–50.

Hoskin P.W.O. & Schaltegger U. 2003: The composition of zircon and igneous and metamorphic petrogenesis. In: Hanchar J.M. & Hoskin P.W.O. (Eds.): Zircon. *Mineral. Soc. Amer.; Geochem. Soc. Rev. Miner. Geochem.,* Washington 53, 27–62.

Hutchison C.S. 1974: Laboratory handbook of petrographic techniques. *John Wiley & Sons*, New York, 1–527.

Hutchison C.S. 1975: The norm, its variations, their calculation and relationships. *Schweiz. Mineral. Petrogr. Mitt.* 55, 243–256.

Jain N. & Warnes G.R. 2006: Ballon plot. *R News* 6, 35–38.

Janoušek V. 2006: *Saturnin*, R language script for application of accessory-mineral saturation models in igneous geochemistry. *Geol. Carpathica* 57, 131–142.

Janoušek V., Farrow C.M. & Erban V. 2006: Interpretation of whole-rock geochemical data in igneous geochemistry: introducing Geochemical Data Toolkit (GCDkit). *J. Petrology* 47, 1255–1259.

Janoušek V., Rogers G., Bowes D.R. & Vaňková V. 1997: Cryptic trace-element variation as an indicator of reverse zoning in a granitic pluton: the Říčany granite, Czech Republic. *J. Geol. Soc., London* 154, 807–815.

Janoušek V., Bowes D.R., Braithwaite C.J.R. & Rogers G. 2000a: Microstructural and mineralogical evidence for limited involvement of magma mixing in the petrogenesis of a Hercynian high-K calc-alkaline intrusion: the Kozárovice granodiorite, Central Bohemian Pluton, Czech Republic. *Trans. Roy. Soc. Edinb., Earth Sci.* 91, 15–26.

Janoušek V., Bowes D.R., Rogers G., Farrow C.M. & Jelínek E. 2000b: Modelling diverse processes in the petrogenesis of a composite batholith: the Central Bohemian Pluton, Central European Hercynides. *J. Petrology* 41, 511–543.

Janoušek V., Braithwaite C.J.R., Bowes D.R. & Gerdes A. 2004: Magma-mixing in the genesis of Hercynian calc-alkaline granitoids: an integrated petrographic and geochemical study of the Sázava intrusion, Central Bohemian Pluton, Czech Republic. *Lithos* 78, 67–99.

Johannsen A. 1932, 1937, 1938, 1939: A descriptive petrography of the igneous rocks. *University of Chicago Press*.

Katzer F. 1888: Geologische Beschreibung der Umgebung von Říčan. *Jb. Geol. Reichsanst.* 38, 355–417.

Kodymová A. & Vejnar Z. 1974: Accessoric heavy minerals in plutonic rocks of the Central Bohemian Pluton. [Akcesorické těžké minerály v hlubinných horninách středočeského plutonu.] *Sbor. Geol. Věd, ložisk. Geol. Mineral.* 16, 89–128 (in Czech).

Kretz R. 1983: Symbols for rock-forming minerals. *Amer. Mineralogist* 68, 277–279.

Laube N., Hergarten S. & Neugebauer H.J. 1996: MODUSCALC — a computer program to calculate mode from a geochemical rock analysis. *Comput. and Geosci.* 22, 631–637.

Le Maitre R.W. 1981: GENMIX — a generalized petrological mixing model program. *Comput. and Geosci.* 7, 229–247.

Le Maitre R.W. 2002: Igneous rocks: a classification and glossary of terms: recommendations of the International Union of Geological Sciences, subcommission on the systematics of igneous rocks. *Cambridge University Press*, 1–236.

Madsen I.C. & Scarlett N.V.Y. 2009: Quantitative phase analysis. In: Dinnebier R.E. & Bilinge S.J.J. (Eds.): Powder diffraction: Theory and practise. *RCS Publishing*, Cambridge, 298–331.

Marshall D.J. 1988: Cathodoluminescence of geological materials. *Unwin Hyman*, Boston, 1–145.

Mielke P. & Winkler H.G.F. 1979: Eine bessere Berechnung der Mesonorm für granitische Gesteine. *Neu. Jb. Mineral., Mh.,* 471–480.

Miller C.F. & Mittlefehldt D.W. 1984: Extreme fractionation in felsic magma chambers; a product of liquid-state diffusion or fractional crystallization? *Earth Planet. Sci. Lett.* 68, 151–158.

Minařík L. & Houdková Z. 1986: Element distribution during the weathering of granitic rocks and formation of soils in the area of the massif of Říčany. [Distribuce prvků při zvětrávání hornin a tvorbě půd v oblasti říčanského masívu.] *Acta Montana* 74, 59–78 (in Czech, with English summary).

Minařík L. & Kvídová O. 1986: Fractionation of rare earth elements during weathering of rocks. [Frakcionace vzácných zemin při zvětrávání hornin.] *Acta Montana* 72, 63–74 (in Czech, with English summary).

Minařík L., Žigová A., Bendl J., Skřivan P. & Šťastný M. 1998: The behaviour of rare-earth elements and Y during the rock weathering and soil formation in the Říčany granite massif, Central Bohemia. *Sci. Total Environ.* 215, 101–111.

Minařík L., Skřivan P., Novák J.K., Fottová D. & Navrátil T. 2003: Distribution, cycling and impact of selected inorganic contaminants in ecosystem of the Lesní potok catchment, the Czech Republic. *Ekologia,* Bratislava 22, 305–322.

Mittlefehldt D.W. & Miller C.F. 1983: Geochemistry of the Sweetwater Wash Pluton, California; implications for "anomalous" trace element behavior during differentiation of felsic magmas. *Geochim. Cosmochim. Acta* 47, 109–124.

Montel J.M. 1993: A model for monazite/melt equilibrium and application to the generation of granitic magmas. *Chem. Geol.* 110, 127–146.

Navrátil T. 2003: Biogeochemistry of the II.A group elements in a forested catchment. *Unpublished Ph.D. Thesis, Charles University in Prague*, 1–113.

Navrátil T., Skřivan P., Minařík L. & Žigová A. 2002: Beryllium geochemistry in the Lesní Potok Catchment (Czech Republic), 7 years of systematic study. *Aquat. Geochem.* 8, 121–133.

Navrátil T., Vach M., Skřivan P., Mihaljevič M. & Dobešová I. 2004: Deposition and fate of lead in a forested catchment, Lesní potok, Central Czech Republic. *Water Air Soil Poll., Focus* 4, 619–630.

Navrátil T., Shanley J.B., Skřivan P., Krám P., Mihaljevič M. & Drahota P. 2007: Manganese biogeochemistry in a Central Czech Republic catchment. *Water Air Soil Poll.* 186, 149–165.

Němec D. 1978: Genesis of aplite in the Říčany massif, central Bohemia. *Neu. Jb. Mineral., Abh.* 132, 322–339.

Niggli P. 1931: Die quantitative mineralogische Klassifikation der Eruptivgesteine. *Schweiz. Mineral. Petrogr. Mitt.* 11, 296–364.

Orlov A. 1933: Contribution to the petrography of the Central Bohemian Granite Massif (the Říčany-Benešov-Milevsko-Písek region). [Příspěvek k petrografii středočeského žulového masívu (Říčansko–Benešovsko–Milevsko-Písecko).] *Věst. St. Geol. Úst. Čs. Repl.* 9, 135–144 (in Czech).

Paktunc A.D. 1998: MODAN: an interactive computer program for estimating mineral quantities based on bulk composition. *Comput. and Geosci.* 24, 425–431.

Palivcová M. 1965: The Central Bohemian Pluton — a petrographic review and an attempt at a new genetic interpretation. *Krystalinikum* 3, 99–131.

Palivcová M., Waldhausrová J., Ledvinková V. & Fatková J. 1992: Říčany granite (Central Bohemian Pluton) and its ocelli- and ovoids-bearing mafic enclaves. *Krystalinikum* 21, 33–66.

Pivec E. 1970: On the origin of phenocrysts of potassium feldspars in some granitic rocks of the Central Bohemian Pluton. *Acta Univ. Carol, Geol.* 1970, 11–25.

Pivec E. 1969: Residues of surface kaolinization in granite of Říčany. [Relikty povrchové kaolinizace v říčanské žule.] *Čas. Mineral. Geol.* 14, 61–67 (in Czech, with English summary).

Potts P.J. 1987: A handbook of silicate rock analysis. *Blackie & Son Ltd.*, Glasgow and London, 1–622.

Robie R.A., Bethke P.M. & Beardsley K.M. 1967: Selected X-ray crystallographic data, molar volumes, and densities of minerals and related substances. *U.S. Geol. Surv. Bull. 1248*, Washington, 1–87.

Sawka W.N. 1988: REE and trace element variations in accessory minerals and hornblende from the strongly zoned McMurry Meadows Pluton, California. *Trans. Roy. Soc. Edinb., Earth Sci.* 79, 157–168.

Steinocher V. 1950: The position of some plutonic and dike rocks of the plutonic mass of Central Bohemia in P. Niggli's quantitative mineralogical and chemical system. Part I. *Sbor. St. Geol. Úst. Čs. Rep.,Odd. Geol.* 17, 721–764.

Steinocher V. 1953: The position of some plutonic and dyke rocks of the Pluton of Central Bohemia in P. Niggli's quantitative mineralogical and chemical system. Part II. *Sbor. Ústř. Úst. Geol., Odd. Geol.* 20, 241–288.

Streckeisen A. 1974: Classification and nomenclature of plutonic rocks. *Geol. Rdsch.* 63, 773–786.

Streckeisen A. & Le Maitre R.W. 1979: A chemical approximation to the modal QAPF classification of the igneous rocks. *Neu. Jb. Mineral., Abh.* 136, 169–206.

Taylor S.R. & McLennan S.M. 1995: The geochemical evolution of the continental crust. *Rev. Geophys.* 33, 241–265.

Trubač J., Žák J., Chlupáčová M. & Janoušek V. 2009: Magnetic fabric of the Říčany granite, Bohemian Massif: a record of helical magma flow? *J. Volcanol. Geotherm. Res.* 181, 25–34.

Wark D.A. & Miller C.F. 1993: Accessory mineral behavior during differentiation of a granite suite: monazite, xenotime and zircon in the Sweetwater Wash pluton, southeastern California, U.S.A. *Chem. Geol.* 110, 49–67.

Watson E.B. & Harrison T.M. 1983: Zircon saturation revisited: temperature and composition effects in a variety of crustal magma types. *Earth Planet. Sci. Lett.* 64, 295–304.

Wright T.L. & Doherty P.C. 1970: A linear programming and least squares computer method for solving petrologic mixing problems. *Geol. Soc. Amer. Bull.* 81, 1995–2008.

Žák J., Verner K., Janoušek V., Holub F.V., Kachlík V., Finger F., Hajná J., Tomek F., Vondrovic L. & Trubač J. (2014): A plate-kinematic model for the assembly of the Bohemian Massif constrained by structural relationships around granitoid plutons. In: Schulmann K., Martínez Catalán J.R., Lardeaux J.M., Janoušek V. & Oggiano G. (Eds.): The Variscan orogeny: Extent, timescale and the formation of the European Crust. *Geol. Soc. London, Spec. Publ.* 405, 169–196. Doi: 10.1144/SP405.9

Electronic supplement

JANOUŠEK et al.: Distribution of elements among minerals of a single (muscovite-) biotite granite sample — an optimal approach and general implications

Appendix 1

Analytical techniques

Sampling

The whole-rock sample Žer-1 (~30 kg) was collected in the Žernovka quarry, ca. 850 m NNW of the namesake village off the pluton's center (Fig. 1c, GPS 50°0′22.64″ N; 14°44′56.13″ E). Its bulk was crushed by a steel jaw crusher, homogenized and ground in an agate mill at the Laboratories of the Institute of Geology, Czech Academy of Sciences, v.v.i. (CAS).

Mineral separation

The crushed material (<500 μm) was floated on a Wilfley shaking table. The heavy fraction was filtered on glass frit, rinsed with ethanol and air dried. The light fraction was dried at 105 °C and was used for separation of the main rock-forming minerals. The fraction between 63 and 250 μm thereof served for magnetic separation of biotite. The biotite separate was finally cleaned in acetylene tetrabromide with density of 2.54 $kg \cdot m^{-3}$.

The quartz separate was obtained after biotite separation by flotation using ANP1 (amino nitro paraffin) agent. K-feldspar was separated in bromoform solution (2.59 $kg \cdot m^{-3}$). The material with density greater than 2.54 $kg \cdot m^{-3}$ was plagioclase. Following the separation of quartz and orthoclase, muscovite separation was achieved in bromoform with density 2.74–2.84 $kg \cdot m^{-3}$. Kaolinite was isolated by centrifugation of the fine fraction (<25 μm) in bromoform.

The dried heavy fraction from the shaking table was sieved on a 315 μm nylon sieve. The fine fraction was used for separation of heavy minerals — zircon and monazite. Apatite was recovered from the heavy fraction by centrifugation in methyleniodide with density 3.18–3.25 $kg \cdot m^{-3}$. Magnetite was obtained from the dark part of the heavy fraction by magnetic separation with the intensity of magnetic field set to 0.2 A.

Electron microprobe and BSE imaging

The analyses of the major rock-forming and selected accessory minerals were done with a fully automated CAMECA SX-100 electron microprobe, employing Φ(ρz) correction procedure (Merlet 1992) at the CAS. All analyses were performed at an acceleration voltage of 15 kV but with different beam currents and spot sizes chosen according to the mineral type. Thus 20–40 nA and a spot size of 10 μm were employed for analyses of apatite, titanite, rutile, monazite, magnetite, ilmenite and zircon–thorite solid solution. For feldspars, micas and quartz, the beam current was 10–15 nA and spot size 2 μm. Minor-element interferences have been checked routinely and corrected for by measuring the corresponding standards. All the mineral abbreviations are after Kretz (1983).

Whole-rock major- and minor-element analyses

The major-element whole-rock analysis of the whole-rock sample was undertaken by wet chemistry in the laboratories of the Czech Geological Survey, Prague — Barrandov. Further analytical details are given in Dempírová (2010); the relative 2 σ uncertainties were better than 1 % (SiO_2), 2 % (FeO), 5 % (Al_2O_3, K_2O and Na_2O), 7 % (TiO_2, MnO, CaO), 6 % (MgO) and 10 % (Fe_2O_3, P_2O_5). Interpretation and plotting of the whole-rock geochemical data was done by the R-language package *GCDkit* (Janoušek et al. 2006).

Trace-element analyses

Solution ICP-MS analyses

The trace-element analyses of mineral separates and whole-rock samples were carried out after modified total digestion in mineral acids ($HF + HClO_4$) and borate fusion ($Na_2CO_3 + Na_2B_4O_7$) in Pt crucibles followed by solution nebulization ICP-MS PQ3 VG Elemental at Charles University in Prague. All the chemicals involved were reagent grade (Merck, Germany) and the acids were double distilled. Deionized water from a Millipore system (Milli-Q Academic, USA) was used for all dilutions.

The measured data were processed on-line using VG PlasmaLab software, applying corrections for instrumental drift. The analytical precision for all the elements analysed ranged from 0.5 to 5 % relative. The accuracy of this analytical method was checked using the G-2 and BCR-2 reference materials (USGS, USA). Trace-element ICP-MS analyses followed the methods of Strnad et al. (2005).

In-situ laser ablation analyses

In-situ trace-element analyses were performed on a quadrupole-based ICP-MS Thermo Fisher X-Series II (Charles University) coupled to a NewWave UP 213 laser microprobe (NewWave Research; USA) operating at output wavelength of 213 nm. All samples were prepared as polished thin sections. The data were acquired in the time-resolved and peak jumping mode with one point measured per mass peak and processed off-line by Thermo Fisher PlasmaLab software 2.5.11 321. The raster pattern was linear, approximately

80×400 μm. External calibration of the laser-ablation analyses was done using standards NIST 610 and 612 (Pearce et al. 1997). For internal standardization ^{29}Si concentrations based on electron microprobe measurements were applied. Data reduction included correction for the gas blank, the internal standard and a calibration check; the data were processed off-line in a MS Excel spreadsheet-based program. For details on analytical protocol and correction strategy see Strnad et al. (2005).

Modal analyses

Point counting

Point counting was done on a thin section 3×2 cm using a standard optical microscope. The total number of points counted was 4890.

Image analysis of stained rock slab

The rock sample was stained according to the method of Gabriel & Cox (1929). The polished sample surface was exposed to fumes of HF for about 15 min., then treated with a concentrated solution of sodium cobaltinitrite for another 10 min., rinsed and dried. This reaction forms a yellow coating on K-feldspar and white on plagioclase; quartz remains unaffected.

The image analysis was performed on a scanned stained polished rock slab (ca. 17×7 cm). The abundance of mineral phases was estimated on the basis of pixel colour analysis by Quick Photo Micro 2.2 software. Dark–black areas were attributed to biotite, grey and greyish glassy-like colour to quartz, white to plagioclase and yellow to K-feldspar.

Powder X-ray diffraction

A powder sample was prepared by grinding in an agate mill and, subsequently, in an agate mortar. The powder X-ray diffraction pattern was collected in a conventional Bragg-Brentano geometry on the Philips X'Pert diffractometer equipped with graphite secondary monochromator. The CuK_α radiation was used. To minimize the background, the sample was placed on a flat low-background silicon wafer. Data were acquired in the angular range 3–90° 2Θ, with a step interval of 0.02° and a step-counting time of 9 s. A divergence slit of 0.5° and a receiving slit of 0.1 mm were used.

The quantitative phase analysis of the sample was performed using the Rietveld method (Young 2000). Refinement was done by minimizing the sum of the weighted squared differences between observed and calculated intensities at every 2Θ step in a powder diffraction pattern (Bish & Post 1993). Quartz, orthoclase, plagioclase (albite), biotite and kaolinite were detected in the P-XRD pattern. The Rietveld refinement was performed using the FullProf program (Rodríguez-Carvajal 2006). The structure models used in the refinement were as follows: quartz (Le Page & Donnay 1976), orthoclase (Prince et al. 1973), albite (Ferguson et al. 1958), biotite (Brigatti & Davoli 1990) and kaolinite (Bish & Von Dreele 1989). The structural model of oligoclase instead of albite was also tested in Rietveld refinements, however the differences in the profile agreement factors between both Rietveld fits were insignificant. The differences in the estimated modal composition were below 0.1 wt. %. The background was determined by linear interpolation between consecutive breakpoints in the powder pattern. The pseudo-Voigt function was employed to generate the line shape of the diffraction peaks. The refinement involved the scale factor for each phase, unit-cell parameters for each phase except albite, peak-width parameters for each phase, two asymmetry parameters for biotite and 2Θ zero error. Atomic coordinates, overall isotropic displacement factors, and site occupancy parameters were fixed during the refinement for all phases. The unit-cell parameters of albite were also fixed, since their refinement caused divergence of the fit. The March-Dollase correction for preferred orientation was applied. The [001] direction was used for biotite, kaolinite, feldspar and plagioclase. The refinement converged to the values of the profile agreement factors R_p = 8.9 % and R_{wp} = 11.4 %.

Principles of the least-squares calculations

The least-squares method is employed to solve an overdetermined set of linear algebraic equations, which occur where there are more independent equations than variables (Bryan et al. 1969). Given a matrix A and a vector y, we want to know the vector x that fulfils.

$$y = Ax \quad (1)$$

Our estimate of the vector x should also be chosen so that the computed and real elements of the vector y differ as little as possible.

$$y' = Ax' \quad (2)$$

The squares of these differences are commonly minimized (so-called least-squares method: Bryan et al. 1969; Albarède 1995):

$$R^2 = |y' - y|^2 \quad (3)$$

$$R^2 = \min \quad (4)$$

and the sum of squared residuals is taken as the measure of the goodness of fit. Albarède (1995) discussed in a detail all the necessary mathematical apparatus that is behind the solution. Moreover, Janoušek & Moyen (in print) provide examples of various types of calculations (including normative calculations using real mineral compositions by the least-squares method) and their implementation into the freeware R language.

In geochemistry we very often examine variables that sum up, for instance, to a unity or 100 %. The least-squares method generally does not produce normalized solutions, in the form of vectors whose components would sum up to a given number. We can define the Lagrange multiplier λ as (Albarède (1995):

$$\lambda = \frac{1 - J^T x}{J^T (A^T A)^{-1} J} \quad (5)$$

where x stands for an ordinary least-squares solution and J is a vector, all elements of which are equal to 1. The constrained least-squares solution is than given by:

$$\hat{x} = x + \lambda (A^T A)^{-1} J \quad (6)$$

References

Albarède F. 1995: Introduction to geochemical modeling. *Cambridge University Press*, Cambridge, 1–543.

Bish D.L. & Post J.E. 1993: Quantitative mineralogical analysis using the Rietveld full-pattern fitting method. *Amer. Mineralogist* 78, 932–940.

Bish D.L. & Von Dreele R.B. 1989: Rietveld refinement of non-hydrogen atomic positions in kaolinite. *Clays and Clay Miner.* 37, 4, 289–296.

Brigatti M.F. & Davoli P. 1990: Crystal-structure refinements of 1 M plutonic biotites. *Amer. Mineralogist* 75, 305–313.

Bryan W.B., Finger L.W. & Chayes F. 1969: Estimating proportions in petrographic mixing equations by least-squares approximation. *Science* 163, 926–927.

Dempírová L. 2010: Evaluation of SiO_2, Na_2O, MgO, K_2O determinations in silicate samples by z-score obtained from nineteen interlaboratory tests. [Zhodnocení stanovení SiO_2, Na_2O, MgO a K_2O v silikátových vzorcích pomocí z-skóre získaných z devatenácti mezilaboratorních porovnávání.] *Zpr. Geol. Výzk. v roce 2009*, 323–326 (in Czech with English summary).

Ferguson R.B., Traill R.J. & Taylor W.H. 1958: The crystal structures of low-temperature and high-temperature albites. *Acta Crystallogr.* 11, 331–348.

Gabriel A. & Cox E.P. 1929: A staining method for the quantitative determination of certain rock minerals. *Amer. Mineralogist* 14, 290–292.

Janoušek V. & Moyen J.F. (in print): Mass balance modelling of magmatic processes in *GCDkit*. In: Kumar S. & Singh R.N. (Eds.): Modelling of magmatic and allied processes. *Soc. Earth Sci., Ser. 83, Springer*, Berlin, 225–238. Doi: 10.1007/978-3-319-06471-0_11

Janoušek V., Farrow C.M. & Erban V. 2006: Interpretation of whole-rock geochemical data in igneous geochemistry: introducing Geochemical Data Toolkit (GCDkit). *J. Petrology* 47, 1255–1259.

Kretz R. 1983: Symbols for rock-forming minerals. *Amer. Mineralogist* 68, 277–279.

Le Page Y. & Donnay G. 1976: Refinement of the crystal structure of low-quartz. *Acta Crystallogr., Sect. B* 32, 2456–2459.

Merlet C. 1992: Accurate description of surface ionization in electron probe microanalysis: an improved formulation. *X-RAY Spectrom.* 21, 229–238.

Pearce N.J.G., Perkins W.T., Westgate J.A., Gorton M.P., Jackson S.E., Neal C.R. & Chenery S.P. 1997: A compilation of new and published major and trace element data for NIST SRM 610 and NIST SRM 612 glass reference materials. *Geostand. Newsl.* 21, 115–144.

Prince E., Donnay G. & Martin R.F. 1973: Neutron diffraction refinement of an ordered orthoclase structure. *Amer. Mineralogist* 58, 500–507.

Rodríguez-Carvajal J. 2006: Full Prof .2k Rietveld profile matching & integrated intensities refinement of X-ray and/or neutron data (powder and/or single-crystal). *Laboratoire Léon Brillouin, Centre d'Etudes de Saclay, Gif-sur-Yvette Cedex, France*.

Strnad L., Mihaljevič M. & Šebek O. 2005: Laser ablation and solution ICP-MS determination of rare earth elements in USGS BIR-1G, BHVO-2G and BCR-2G glass reference materials. *Geost. Geoanal. Res.* 29, 303–314.

Young R.A. 2000: The Rietveld method. *Oxford University Press*, Oxford, 1–312.

Appendix 2

Electron microprobe analyses.

a — Average electron-microprobe data used in mass-balance calculations (wt. %).

	SiO_2	TiO_2	Al_2O_3	FeOt	MnO	MgO	CaO	Na_2O	K_2O	P_2O_5
WR	70.34	0.36	14.64	1.5	0.024	1.14	1.36	3.71	5.55	0.15
Qtz	99.86	n.d.	0.02	n.d.	n.d.	n.d.	n.d.	n.d.	n.d.	n.d.
Or	64.16	n.d.	18.47	0.03	0.034	n.d.	0.01	0.96	15.61	0.01
Pl	62.97	n.d.	20.07	n.d.	n.d.	0.01	3.95	9.2	0.44	0.02
Bt	37.5	3.33	14.8	17.26	0.24	13.35	0.04	0.14	9.47	n.d.
Ms	49.38	0.27	31.26	3.72	0.05	0.98	0.12	0.27	9.79	n.d.
Kln	45.59	0.91	39.84	0.02	0.01	n.d.	n.d.	n.d.	n.d.	0.03
Ilm	0.01	50.32	n.d.	42.71	3.091	n.d.	n.d.	n.d.	n.d.	0.01
Ttn	30.49	35.77	2.79	1.11	0.092	n.d.	27.58	n.d.	n.d.	0.01
Ap	0.04	0.01	n.d.	0.03	0.161	n.d.	55.98	n.d.	n.d.	42.68
Mgt	n.d.	n.d.	n.d.	n.d.	0.233	n.d.	n.d.	n.d.	n.d.	n.d.
Mnz	2.42	n.d.	n.d.	0.04	n.d.	n.d.	0.37	n.d.	n.d.	25.61
Zrn	31.1	n.d.	0.29	0.44	0.006	n.d.	0.14	n.d.	n.d.	n.d.
Rt	0.28	97.35	n.d.	1.59	0.031	n.d.	0.08	n.d.	n.d.	n.d.

n.d. — not detected.

b — Typical analyses for the main and accessory minerals (wt. % and apfu).

	Feldspars			Biotite		Magnetite	
ID	**Plg15T**	**Plg19T**	**16T**	**ID**	**Bt14**	**ID**	**Mgt1**
SiO_2	63.75	66.44	64.26	SiO_2	37.50	SiO_2	0.03
TiO_2	n.d.	0.01	n.d.	TiO_2	3.33	TiO_2	0.01
Al_2O_3	22.00	20.33	18.29	Al_2O_3	14.80	Al_2O_3	0.04
FeOt	n.d.	n.d.	0.02	FeOt	16.95	FeOt	95.55
MnO	0.02	n.d.	n.d.	MnO	0.24	MnO	1.17
MgO	0.009	n.d.	0.01	MgO	13.35	MgO	n.d.
CaO	3.59	1.72	0.03	CaO	0.04	CaO	0.01
Na_2O	9.72	10.84	1.30	Na_2O	0.14	Na_2O	n.d.
K_2O	0.38	0.21	15.48	K_2O	9.47	K_2O	n.d.
P_2O_5	0.013	0.009	0.008	H_2O+	2.44	P_2O_5	n.d.
Total	99.46	99.61	99.39	F	1.66	ThO_2	n.d.
Si apfu	2.834	2.930	2.987	Total	99.92	U_2O_3	n.d.
Ti	0.000	0.000	0.000	Si apfu	2.812	Y_2O_3	n.d.
Al	1.153	1.057	1.002	Al(IV)	1.188	TR_2O_3	n.d.
Fe	0.000	0.000	0.001	Σ	4.000	Total	96.81
Mn	0.001	0.000	0.000	Al(VI)	0.121	Si apfu	0.004
Mg	0.001	0.000	0.001	Ti	0.188	Ti	0.001
Ca	0.171	0.081	0.002	Fe	1.063	Al	0.005
Na	0.838	0.927	0.117	Mn	0.015	Fe^{2+}	0.964
K	0.021	0.012	0.918	Mg	1.492	Fe^{3+}	1.995
P	0.000	0.000	0.000	Σ	2.879	Mn	0.037
O	8.000	8.000	8.000	Ca	0.003	Mg	0.000
An mol. %	16.6	8.0	0.1	Na	0.020	Ca	0.000
Ab	81.3	90.9	8.5	K	0.906	Na	0.000
Or	2.1	1.2	91.4	Σ	0.930	K	0.000
				F	0.394	P	0.000
				OH*	1.606	Th	0.000
				XMg	0.58	U	0.000
				XFe	0.42	Y	0.000

n.d. — not detected, n.a. — not analysed.

	Zircon			Monazite		Rutile	Titanite
ID	**Zrn5**	**Zrn7**	**Zrn10**	**Mnz8**	**Mnz9**	**Rt1**	**Ttn4**
SiO_2	32.08	31.10	32.27	1.89	2.42	0.51	30.30
TiO_2	0.02	n.d.	n.d.	0.01	0.00	98.82	36.32
Al_2O_3	0.06	0.29	n.d.	n.d.	n.d.	0.01	2.44
P_2O_5	n.d.	n.d.	n.d.	26.61	25.61	0.00	0.02
FeO	0.14	0.44	0.05	0.00	0.04	0.46	n.a.
Fe_2O_3	n.a.	n.a.	n.a.	n.a.	n.a.	n.a.	1.08
MnO	n.d.	0.01	n.d.	0.12	n.d.	n.d.	0.11
CaO	0.02	0.14	n.d.	0.41	0.37	0.10	27.23
Y_2O_3	n.d.	0.39	0.11	0.55	0.40	0.06	0.36
ZrO_2	63.28	61.21	62.89	n.a.	n.a.	n.a.	n.a.
HfO_2	1.87	1.89	1.30	n.a.	n.a.	n.a.	n.a.
Ce_2O_3	n.d.	n.d.	0.04	32.74	32.78	0.14	0.50
La_2O_3	0.13	0.07	n.d.	15.07	14.51	n.d.	0.07
Nd_2O_3	n.d.	n.d.	0.08	9.35	8.66	n.d.	0.60
Pr_2O_3	0.12	0.10	n.d.	2.87	2.86	0.04	0.23
Sm_2O_3	0.00	0.09	0.04	1.07	1.18	0.00	0.02
Eu_2O_3	0.01	0.02	0.01	n.d.	n.d.	0.05	n.d.
Gd_2O_3	0.02	0.04	0.01	0.48	0.37	n.d.	0.15
Tb_2O_3	n.d.	n.d.	n.d.	0.08	0.03	n.d.	0.08
Dy_2O_3	0.01	0.01	0.04	0.04	n.d.	0.01	0.08
Ho_2O_3	n.d.	0.01	0.03	0.01	0.01	0.04	0.02
Er_2O_3	0.00	0.02	0.00	0.05	0.02	0.00	0.03
Tm_2O_3	n.d.	n.d.	n.d.	0.08	0.09	0.02	0.02
Yb_2O_3	n.d.	n.d.	0.04	n.d.	0.03	0.02	0.01
Lu_2O_3	n.d.	n.d.	n.d.	n.d.	n.d.	0.00	n.d.
ThO_2	0.13	0.17	0.03	8.18	10.42	0.02	0.02
U_2O_3	0.18	0.20	0.60	0.50	0.37	0.03	0.01
Total	98.05	96.19	97.54	100.110	100.144	100.322	99.66
Si apfu	1.007	0.998	1.015	0.077	0.099	0.007	1.001
Ti	0.000	0.000	0.000	0.000	0.000	0.988	0.903
Al	0.002	0.011	0.000	0.000	0.000	0.000	0.095
P	0.000	0.000	0.000	0.912	0.887	0.000	0.001
Fe^{2+}	0.004	0.012	0.001	0.000	0.001	0.005	n.a.
Fe^{3+}	n.a.	n.a.	n.a.	n.a.	n.a.	n.a.	0.027
Mn	0.000	0.000	0.000	0.004	0.000	0.000	0.003
Ca	0.001	0.005	0.000	0.018	0.016	0.001	0.964
Y	0.000	0.007	0.002	0.012	0.009	0.000	0.006
Zr	0.968	0.958	0.965	n.a.	n.a.	n.a.	n.a.
Hf	0.017	0.017	0.012	n.a.	n.a.	n.a.	n.a.
Ce	0.000	0.000	0.000	0.485	0.491	0.001	0.006
La	0.001	0.001	0.000	0.225	0.219	0.000	0.001
Nd	0.000	0.000	0.001	0.135	0.127	0.000	0.007
Pr	0.001	0.001	0.000	0.042	0.043	0.000	0.003
Sm	0.000	0.001	0.000	0.015	0.017	0.000	0.000
Eu	0.000	0.000	0.000	0.000	0.000	0.000	0.000
Gd	0.000	0.000	0.000	0.006	0.005	0.000	0.002
Tb	0.000	0.000	0.000	0.001	0.000	0.000	0.001
Dy	0.000	0.000	0.000	0.000	0.000	0.000	0.001
Ho	0.000	0.000	0.000	0.000	0.000	0.000	0.000
Er	0.000	0.000	0.000	0.001	0.000	0.000	0.000
Tm	0.000	0.000	0.000	0.001	0.001	0.000	0.000
Yb	0.000	0.000	0.000	0.000	0.000	0.000	0.000
Lu	0.000	0.000	0.000	0.000	0.000	0.000	0.000
Th	0.001	0.001	0.000	0.075	0.097	0.000	0.000
U	0.001	0.001	0.004	0.005	0.003	0.000	0.000
A	0.995	1.005	0.988	1.020	1.024		
B	1.009	1.009	1.015	0.988	0.986		
Sum cat.	2.004	2.014	2.003	2.015	2.016	1.004	3.021

Appendix 3: Laser-ablation ICP-MS data for the main rock forming minerals (ppm).

LA ICP-MS		Quartz										
DL (LA)	ppm	q1	q2	q3	q4	q1	q2	q3	q4	q1	Avg	SD
0.01	Be	0.08	0.11		0.17	0.03	0.00	0.05	0.00	0.00	0.06	0.06
0.35	Mn	0.12	0.12	0.16	0.10	0.09	0.21	0.22	0.20	0.20	0.16	0.05
0.095	Co	0.01	0.01	0.00	0.01	0.01	0.01	0.03	0.00	0.01	0.01	0.01
1.15	Ni	1.97	1.77	0.94	1.27	2.29	2.17	3.02	2.93	3.12	2.16	0.77
0.48	Zn	0.10	0.22	0.26	0.19	0.11	0.64	0.69	0.69	0.65	0.39	0.26
0.26	Rb	0.03	0.05	0.05	0.05	0.35	0.08	0.07	0.05	0.09	0.09	0.10
0.085	Sr	0.10	0.16	0.09	0.06	0.12	0.13	0.07	0.13	0.12	0.11	0.03
0.045	Y	0.00	0.00	0.01	0.05	0.00	0.00	0.00	0.00	0.00	0.01	0.02
0.25	Zr	0.05	0.03	1.31		0.09	0.14	0.06	0.04	0.03	0.22	0.44
0.05	Nb	0.01	0.00	0.00		0.00		0.04		0.01	0.01	0.01
0.23	Cd	0.16	0.08	0.02	0.01	0.11	0.05	0.01	0.01	0.03	0.05	0.05
0.085	Ba	0.19	0.28	0.12	0.13	0.80	0.39	0.36	0.38	0.38	0.34	0.20
0.020	La	0.001	0.009	0.003	0.007	0.001	0.01	0.00	0.00	0.00	0.004	0.00
0.028	Ce	0.008	0.013	0.007	0.021	0.011	0.03	0.00	0.01	0.00	0.012	0.01
0.008	Pr	0.000	0.000	0.000	0.003	0.000	0.00	0.00	0.00	0.00	0.001	0.00
0.083	Nd	0.000	0.000	0.007	0.004	0.003	0.01	0.00	0.00	0.00	0.003	0.00
0.097	Sm	0.000	0.000	0.000	0.000	0.000	0.00	0.00	0.00	0.00	0.000	0.00
0.008	Eu	0.000	0.000	0.000	0.000	0.000	0.00	0.00	0.00	0.00	0.000	0.00
0.032	Gd	0.000	0.000	0.000	0.000	0.000	0.00	0.00	0.00	0.00	0.000	0.00
0.009	Tb	0.000	0.000	0.000	0.000	0.000	0.00	0.00	0.00	0.00	0.000	0.00
0.030	Dy	0.000	0.000	0.000	0.001	0.000	0.00	0.00	0.00	0.00	0.000	0.00
0.004	Ho	0.000	0.000	0.001	0.001	0.000	0.00	0.00	0.00	0.00	0.000	0.00
0.012	Er	0.000	0.000	0.003	0.005	0.000	0.00	0.00	0.00	0.00	0.001	0.00
0.002	Tm	0.000	0.000	0.000	0.001	0.000	0.00	0.00	0.00	0.00	0.000	0.00
0.022	Yb	0.000	0.000	0.000	0.002	0.000	0.00	0.00	0.00	0.00	0.000	0.00
0.003	Lu	0.000	0.000	0.000	0.000	0.000	0.00	0.00	0.00	0.00	0.000	0.00
0.03	Hf	0.00	0.00	0.08		0.00	0.01	0.00	0.00	0.00	0.01	0.03
0.05	Ta	0.01	0.01	0.01		0.01		0.02	0.02	0.02	0.01	0.01
0.21	Pb	0.08	0.07	0.07	0.08	0.11	0.15	0.13	0.12	0.11	0.10	0.03
0.02	Th	0.66	1.01	0.11	0.04	0.35	0.97	0.31		1.13	0.57	0.43
0.011	U	0.01	0.01	0.04	0.11	0.01	0.02	0.02	0.02	0.02	0.03	0.03

DL = detection limit.

	K-feldspar					
	k1	k2	k3	k4	Avg	SD
Be	0.58	0.85	2.15	1.77	1.34	0.74
Mn	2.15	2.44	1.33	1.72	1.91	0.49
Co	0.04	0.07	0.03	0.01	0.04	0.02
Ni	0.60	0.65	0.54	0.19	0.49	0.21
Zn	1.28	1.18	0.97	0.29	0.93	0.45
Rb	323.07	328.94	342.18	337.47	332.91	8.55
Sr	529.10	458.50	390.70	325.38	425.92	87.67
Y	0.07	0.56	0.14	0.10	0.21	0.23
Zr	2.05	5.52	5.23	1.16	3.49	2.21
Nb	0.10	0.13	0.04	0.05	0.08	0.04
Cd	0.06	0.04	0.02	0.04	0.04	0.02
Ba	4104.54	3186.51	1552.54	1134.56	2494.54	1391.38
La	1.76	1.77	1.58	1.49	1.65	0.14
Ce	1.41	2.07	2.61	1.26	1.84	0.62
Pr	0.07	0.17	0.12	0.12	0.12	0.04
Nd	0.14	0.72	0.46	0.44	0.44	0.24
Sm	0.02	0.17	0.08	0.06	0.08	0.06
Eu	1.21	1.07	0.93	0.75	0.99	0.19
Gd	0.02	0.14	0.05	0.04	0.06	0.05
Tb	0.00	0.02	0.00	0.00	0.01	0.01
Dy	0.01	0.09	0.02	0.02	0.03	0.04
Ho	0.00	0.01	0.00	0.00	0.00	0.01
Er	0.00	0.04	0.02	0.00	0.02	0.02
Tm	0.00	0.01	0.00	0.00	0.00	0.00
Yb	0.00	0.03	0.02	0.01	0.01	0.01
Lu	0.00	0.01	0.00	0.00	0.00	0.00
Hf	0.09	0.13	0.14	0.03	0.10	0.05
Ta	0.04	0.04	0.03	0.03	0.04	0.01
Pb	121.45	107.57	121.25	115.96	116.56	6.51
Th	0.14	0.16	0.23	0.07	0.15	0.07
U	0.10	0.28	0.25	0.83	0.36	0.32

	Plagioclase				Excluded from calculation			
	p1	p2	Avg	SD	p3	p4	p5	
Be	19.66	23.66	21.66	2.83	17.25	18.36	22.67	
Mn	77.23	33.80	55.52	30.71	47.62	40.88	56.09	
Co	2.29	0.92	1.61	0.97	1.28	0.77	1.54	
Ni	2.90	1.35	2.12	1.10	3.29	2.22	2.33	
Zn	18.12	7.98	13.05	7.17	10.68	6.73	12.87	
Rb	268.20	46.29	157.25	156.91	154.30	101.40	90.50	
Sr	499.30	500.80	500.05	1.06	524.90	606.90	512.70	
Y	0.13	0.16	0.15	0.02	0.66	0.57	5.25	
Zr	16.53	3.90	10.21	8.93	14.43	6.36	293.40	
Nb	9.51	1.60	5.55	5.59	0.24	1.77	1.47	
Cd	0.07	0.04	0.06	0.02	0.10	0.03	0.11	
Ba	213.10	57.97	135.54	109.69	104.40	111.10	72.53	
La	20.43	27.00	23.72	4.65	213.50	326.80	54.60	inclusions of Mnz, Ap?
Ce	36.29	40.69	38.49	3.11	283.30	356.50	129.40	
Pr	3.94	5.47	4.71	1.09	40.92	51.38	10.52	
Nd	11.22	13.24	12.23	1.43	125.50	159.00	34.09	
Sm	0.57	0.88	0.73	0.22	6.80	8.76	3.22	
Eu	0.60	0.84	0.72	0.17	1.12	1.32	1.05	
Gd	0.59	0.57	0.58	0.01	4.45	5.88	2.33	
Tb	0.02	0.03	0.024	0.01	0.18	0.25	0.22	
Dy	0.03	0.05	0.037	0.01	0.27	0.28	1.05	
Ho	0.00	0.00	0.004	0.00	0.03	0.03	0.21	
Er	0.03	0.03	0.027	0.00	0.17	0.25	0.61	
Tm	0.00	0.00	0.001	0.00	0.01	0.01	0.10	
Yb	0.01	0.00	0.007	0.01	0.03	0.03	0.80	
Lu	0.00	0.00	0.001	0.00	0.00	0.00	0.12	
Hf	0.95	0.20	0.58	0.53	0.63	0.19	7.68	
Ta	0.09	0.02	0.05	0.05	0.02	0.18	0.03	
Pb	62.66	58.04	60.35	3.27	78.75	78.32	76.86	
Th	4.90	1.34	3.12	2.52	14.98	8.14	21.04	
U	1.97	1.35	1.66	0.44	10.26	10.11	8.87	

	Biotite				
	B1	B2	B3	Avg	SD
Be	4.481	5.162	4.468	4.70	0.40
Mn	1357.579	1380.579	1358.579	1365.58	13.00
Co	24.955	24.765	23.835	24.52	0.60
Ni	109.12	119.72	117.52	115.45	5.59
Zn	259.247	263.847	256.847	259.98	3.56
Rb	828.107	756.107	633.507	739.24	98.39
Sr	1.395	1.844	1.951	1.73	0.30
Y	0.053	4.416	4.036	2.84	2.42
Zr	0.915	2.243	0.567	1.24	0.88
Nb	91.419	95.239	124.999	103.89	18.38
Cd	0.079	0.096	0.005	0.06	0.05
Ba	1114.197	1186.197	1458.197	1252.86	181.43
La	0.031	0.801	0.901	0.58	0.48
Ce	0.03	2.372	2.756	1.72	1.48
Pr	0.001	0.623	0.568	0.40	0.34
Nd	0.003	3.189	3.232	2.14	1.85
Sm	0.001	1.139	1.017	0.72	0.62
Eu	0.054	0.103	0.132	0.10	0.04
Gd	0	0.915	0.918	0.61	0.53
Tb	0	0.139	0.124	0.09	0.08
Dy	0.002	0.733	0.695	0.48	0.41
Ho	0.001	0.134	0.141	0.09	0.08
Er	0.004	0.281	0.282	0.19	0.16
Tm	0	0.037	0.034	0.02	0.02
Yb	0.001	0.243	0.186	0.14	0.13
Lu	0.001	0.028	0.025	0.02	0.01
Hf	0.115	0.141	0.028	0.09	0.06
Ta	6.912	9.562	14.066	10.18	3.62
Pb	2.832	3.554	3.959	3.45	0.57
Th	0.076	0.709	0.534	0.44	0.33
U	0.027	0.133	0.086	0.08	0.05

Appendix 4

Trace-element composition of the whole-rock, individual rock-forming and accessory minerals determined by the ICP-MS technique (ppm).

ppm	WR	Qtz	Qtz	Kfs	Kfs	Pl	Pl	Bt	Bt	Ms	Kln	Ilm	Ttn	Ap	Mgt	Mnz	Zrn	Rt
	wet[1]	LA[2]	wet	wet	LA	LA	wet	LA	wet	wet	wet	wet	wet	wet	wet	wet	wet	wet
Rb	**266.56**	0.09	11.71	536.58	332.91	157.25	101.71	739.24	1179.96	617.99	45.16	14.78	1.92	0.55	19.75	3.88	25.72	0.63
Sr	**387.27**	0.11	27.19	458.72	425.92	500.05	520.24	1.73	14.74	178.81	14.66	12.58	34.11	150.48	14.81	103.73	46.38	31.03
Ba	**1122.41**	0.34	52.77	2852.66	2494.54	135.54	764.91	1252.86	1058.16	1114.74	17.83	26.17	8.63	1.93	25.01	18.74	267.48	157.93
Be	**10.38**	0.06	1.08	5.53	1.34	21.66	21.35	4.70	5.50	7.40	9.90	4.81	6.61	1.40	2.76	25.40	97.00	1.92
U	**9.61**	0.03	3.01	2.99	0.36	1.66	5.08	0.08	29.02	59.31	1.80	100.40	116.40	24.73	32.82	403.65	489.30	620.25
Th	**24.36**	0.57	8.28	6.45	0.15	3.12	13.42	0.44	69.99	485.63	6.09	72.80	346.15	7.32	113.40	3836.40	950.53	2158.54
Pb	**63.28**	0.10	5.59	124.73	116.56	60.35	56.10	3.45	23.41	50.69	84.00	352.15	315.93	54.30	75.60	1101.00	150.00	315.52
Zr	**169.91**	0.22	56.83	65.16	3.49	10.21	96.48	1.24	647.91	687.74	78.37	1574.23	10081.73	1.20	980.73	10086.73	453122[3]	44550.43
Hf	**5.46**	0.01	1.82	2.05	0.10	0.58	3.10	0.09	21.72	25.72	3.73	48.69	278.46	0.66	30.50	307.86	16010[3]	1361.33
Nb	**16.04**	0.01	1.02	1.36	0.08	5.55	2.94	103.89	178.97	47.20	7.45	79.26	39.74	0.13	35.69	35.31	3288.90	4675.19
Ta	**1.66**	0.01	0.10	0.28	0.04	0.05	0.61	10.18	18.18	19.83	2.36	13.08	9.09	0.05	6.32	4.97	425.15	484.02
La	**24.85**	0.00	6.74	5.98	1.65	23.72	17.35	0.58	41.20	1078.53	34.07	726.72	3555.57	424.51	1088.71	26574.30	496.37	1861.82
Ce	**48.38**	0.01	13.29	10.75	1.84	38.49	31.08	1.72	98.37	1593.25	83.38	1325.86	8572.95	1158.43	1918.03	44278.88	1138.86	2199.46
Pr	**5.37**	0.00	1.47	1.23	0.12	4.71	3.20	0.40	12.36	177.72	9.92	141.69	1219.82	220.99	187.90	4676.15	120.19	519.95
Nd	**19.81**	0.00	5.47	4.64	0.44	12.23	11.01	2.14	52.50	446.35	34.78	417.65	4961.41	1104.99	506.24	13148.31	446.92	2031.71
Sm	**3.47**	0.00	0.98	0.90	0.08	0.73	1.67	0.72	12.06	37.75	8.84	51.27	1199.01	353.17	48.38	1278.54	82.09	282.37
Eu	**0.89**	0.00	0.11	1.19	0.99	0.72	1.12	0.10	0.70	2.71	0.64	3.23	52.55	18.27	1.92	40.79	6.92	7.38
Gd	**2.66**	0.00	0.79	0.76	0.06	0.58	1.46	0.61	9.37	33.80	7.03	30.68	633.40	221.64	31.35	732.12	65.78	201.21
Tb	**0.31**	0.00	0.10	0.09	0.01	0.02	0.16	0.09	1.28	4.76	1.45	3.44	107.44	38.17	3.46	62.70	9.70	18.59
Dy	**1.41**	0.00	0.50	0.47	0.03	0.04	0.73	0.48	6.63	9.27	6.48	16.46	531.87	200.26	15.20	217.73	60.58	76.40
Ho	**0.24**	0.00	0.09	0.09	0.00	0.00	0.13	0.09	1.18	1.48	0.84	2.76	86.80	35.36	2.69	32.37	15.22	15.27
Er	**0.68**	0.00	0.27	0.25	0.02	0.03	0.41	0.19	3.37	6.56	1.98	7.54	212.97	93.23	7.53	90.19	58.75	54.28
Tm	**0.09**	0.00	0.04	0.04	0.00	0.00	0.05	0.02	0.46	0.51	0.21	0.92	25.52	11.83	0.87	9.66	10.83	8.78
Yb	**0.57**	0.00	0.24	0.23	0.01	0.01	0.36	0.14	3.00	3.27	1.36	6.03	140.28	72.22	5.42	56.97	86.87	69.14
Lu	**0.08**	0.00	0.04	0.03	0.00	0.00	0.05	0.02	0.41	0.41	0.16	0.87	14.81	9.30	0.79	6.37	16.32	12.16
Y	**6.65**	0.01	2.46	2.43	0.21	0.15	3.76	2.84	33.98	33.32	16.61	78.31	2173.15	1173.80	69.54	839.34	447.34	398.70
Ni	**14.36**	2.16	0.71	0.34	0.49	2.12	1.59	115.45	136.90	19.81	0.13	6.61	4.82	0.99	80.92	1.81	1252.13	2010.92
Zn	**39.69**	0.39	0.53	1.73	0.93	13.05	6.19	259.98	471.14	99.10	3.08	90.73	95.48	14.21	40.96	92.83	497.63	458.62
Co	**3.52**	0.01	0.13	0.19	0.04	1.61	0.50	24.52	32.95	5.34	0.29	6.49	11.05	0.27	10.01	2.47	58.26	1394.28
Cd	**0.11**	0.05	0.05	0.04	0.04	0.06	0.08	0.06	0.57	4.00	0.13	2.47	4.73	1.05	3.83	5.21	75.11	40.01

[1] – Mineral separates dissolved and analyzed in solution by ICP-MS technique. See text Appendix 1 for analytical details.
[2] – Averaged single-spot analyses as determined by the laser-ablation ICP-MS.
[3] – Electron microprobe; too high to be determined by the ICP-MS.
In grey are shown analyses not taken into consideration. See text for discussion.

Appendix 5

Typical electron-microprobe analyses of the zircon-like ABO_4-type phase (wt. % and apfu).

	1	2	3	4	5	6
SiO_2	16.055	14.810	14.704	15.398	14.739	16.300
TiO_2	0.090	n.d.	0.087	n.d.	0.058	0.034
Al_2O_3	0.667	0.733	0.650	0.642	0.878	0.704
FeO	1.220	2.241	4.426	0.732	6.781	1.002
MnO	0.026	0.132	0.186	0.057	0.439	0.058
MgO	0.101	0.202	0.174	0.186	0.236	0.128
CaO	4.765	4.875	4.612	4.795	4.574	4.641
K_2O	0.137	0.091	0.098	0.086	0.095	0.218
P_2O_5	6.582	6.699	6.684	6.888	6.353	6.407
SO_2	0.149	0.241	0.202	0.188	0.198	0.172
Sc_2O_3	0.021	0.014	0.030	0.003	0.012	0.009
As_2O_3	0.479	0.332	0.285	0.264	0.362	0.483
ZrO_2	27.758	24.869	23.731	26.561	25.640	27.874
HfO_2	0.570	0.569	0.596	0.617	0.571	0.692
Nb_2O_5	n.d.	0.014	0.003	0.017	n.d.	n.d.
SnO	0.010	n.d.	0.029	n.d.	0.036	0.005
PbO	0.214	0.265	0.278	0.296	0.192	0.208
UO_2	1.278	1.106	1.179	1.208	1.240	1.033
ThO_2	31.947	32.353	31.751	35.250	29.028	31.265
Ce_2O_3	3.236	2.377	2.104	2.238	2.058	3.378
SmO	0.122	0.172	0.011	0.061	0.213	0.206
Gd_2O_3	n.d.	n.d.	0.169	0.210	n.d.	0.041
Dy_2O_3	0.170	0.119	0.042	0.067	0.371	0.181
Er_2O_3	n.d.	n.d.	n.d.	n.d.	n.d.	n.d.
Yb_2O_3	0.077	0.099	n.d.	n.d.	n.d.	n.d.
Y_2O_3	0.298	0.215	0.207	0.137	0.219	0.287
F	0.606	0.358	0.345	0.651	0.163	0.681
Total	96.578	92.886	92.583	96.552	94.456	96.007
Si	0.647	0.624	0.622	0.631	0.606	0.658
Ti	0.003	0.000	0.003	0.000	0.002	0.001
Al	0.032	0.036	0.032	0.031	0.043	0.034
Fe	0.041	0.079	0.156	0.025	0.233	0.034
Mn	0.001	0.005	0.007	0.002	0.015	0.002
Mg	0.006	0.013	0.011	0.011	0.014	0.008
Ca	0.206	0.220	0.209	0.210	0.201	0.201
K	0.007	0.005	0.005	0.004	0.005	0.011
P	0.225	0.239	0.239	0.239	0.221	0.219
S	0.006	0.010	0.008	0.007	0.008	0.007
Sc	0.001	0.001	0.001	0.000	0.000	0.000
As	0.012	0.008	0.007	0.007	0.009	0.012
Zr	0.546	0.511	0.489	0.530	0.514	0.549
Hf	0.007	0.007	0.007	0.007	0.007	0.008
Nb	0.000	0.000	0.000	0.000	0.000	0.000
Sn	0.000	0.000	0.001	0.000	0.001	0.000
Pb	0.002	0.003	0.003	0.003	0.002	0.002
U	0.011	0.010	0.011	0.011	0.011	0.009
Th	0.293	0.310	0.305	0.329	0.271	0.287
Ce	0.048	0.037	0.033	0.034	0.031	0.050
Sm	0.002	0.003	0.000	0.001	0.003	0.003
Gd	0.000	0.000	0.002	0.003	0.000	0.001
Dy	0.002	0.002	0.001	0.001	0.005	0.002
Er	0.000	0.000	0.000	0.000	0.000	0.000
Yb	0.001	0.001	0.000	0.000	0.000	0.000
Y	0.006	0.005	0.005	0.003	0.005	0.006
F	0.077	0.048	0.046	0.084	0.021	0.087
site A	0.921	0.917	0.909	0.914	0.886	0.929
site B	1.183	1.210	1.249	1.175	1.321	1.175

The EPMA results are recalculated on the basis of 4O *apfu*.
n.d. — not detected.
Site *B* includes Si, Al, P, As and S, the site *A* comprises all other elemets (except F).